ENVIRONMENTAL RADIATION MEASUREMENTS ON MIR STATION:

FBI-3: Internal Experiment
FBI-4: External Experiment

Final Report

E. V. Benton and A. L. Frank
Physics Research Laboratory
University of San Francisco
2130 Fulton Street
San Francisco, CA 94117-1080

E. R. Benton
Eril Research, Inc.
P. O. Box 150788
San Rafael, CA 94915-0788

Contract No. NCC2-893
NASA-Ames Research Center

5 September 2000

**ENVIRONMENTAL RADIATION MEASUREMENTS
ON MIR STATION:
FBI-3: Internal Experiment
FBI-4: External Experiment**

Final Report

1. INTRODCUTION

1.1 Hypothesis

A series of passive integrating measurements of environmental radiation with dosimeters located inside the Mir Space Station will significantly expand the U. S. data base at the 51.6° inclination orbit, provide detailed information on shielding effects, allow intercomparison of dosimetric methods and provide data for extensive testing of model calculations.

1.2 Abstract

The ionizing radiation environment on the interior and exterior of the Russian Mir Orbital Station was measured using a combination of two types of passive radiation detector. Thermoluminescent detectors (TLDs) were used to measure absorbed dose. CR-39 Plastic Nuclear Track Detectors (PNTDs) were used to measure the LET Spectra ≥5 keV/μm. Results from TLDs and CR-39 PNTDs were combined to determine total dose and dose equivalent. Radiation measurements on the interior of the Mir Orbital Station were carried out using six Area Passive Dosimeters (APDs), four located in the Base Block and two located in the Kvant 2 Module, during the NASA-2/Mir-21, NASA-3/Mir-22 and NASA-4/Mir-23 missions. The radiation environment on the exterior of Mir was measured using an External Dosimeter Array (EDA) mounted on the outer surface of the Kvant 2 module. The external radiation environment and a location inside the Kvant 2 module roughly corresponding to the exterior location of the EDA were monitored for a period of 130 days during the NASA-4/Mir-23 and NASA-5/Mir-24 missions.

Dose rates measured by TLDs and corrected for high-LET efficiency on the interior of Mir ranged from 284 to 420 μGy/day during the NASA-2/Mir-21 mission, from 284 to 436 μGy/day during the NASA-3/Mir-22 mission, and from 304 to 375 μGy/day during the NASA-4/Mir-23 mission. Dose equivalent rates ranged from 518 to 646 μSv/day on the NASA-2/Mir-21 mission, from 626 to 724 μSv/day on the NASA-3/Mir-22 mission and from 624 to 678 μSv/day on the NASA-4/Mir-23 mission. Over the course of the three missions, mean quality factor for the six locations ranged from 1.6 to 2.3. Dose as a function of shielding depth was measured using thin TLD stacks positioned in the EDA. Dose was found to decrease by nearly three orders of magnitude within the first g/cm^2 of shielding. The measured EDA doses ranged from 72.5 Gy under shielding of 0.0146 g/cm^2 to 0.093 Gy under 3.25 g/cm^2 shielding.

1.3 Objectives

The NASA/Mir Phase 1 Science Program can be seen as marking the beginning of the permanent presence of American astronauts in space. Between March 1995 and May 1998, seven American astronauts lived and worked aboard the Russian Mir Space Station for periods of up to nearly seven months. The on-orbit assembly of the International Space Station (ISS) marks another

milestone in the era of a continuous human presence in space. One consequence of the ISS is the increase in the number of personnel in low earth orbit (LEO) at any given time and the increase in the duration of each astronaut's stay in LEO, leading to an increase in the overall radiation exposure received by astronauts. Accurate prediction of accumulated radiation dose and dose equivalent to astronaut crews and the subsequent assessment of risk from long duration radiation exposure has therefore become of greater necessity if the long-term, stochastic effects of space radiation are to be minimized. Dose and dose equivalent prediction and risk assessment are based upon models of the radiation environment in LEO and on models of the transport of radiation through matter. These models are based in part on in-situ measurements of the radiation environment and additional measurements are needed to validate the accuracy of these models. In addition, an understanding of the different constituent components of the radiation environment in LEO is needed to base radiation modeling efforts on an analytical and not merely empirical foundation.

The determination of astronaut risk from environmental radiation on spacecraft in LEO requires accurate measurement of dose from the various types of ionizing particles present. Dose equivalent, the radiation quantity used for risk assessment, is the product of the dose and an empirically determined radiation quality factor based on the evaluated biological effectiveness of the radiation. The quality factor is a function of the Linear Energy Transfer (LET) of the radiation. LET is the amount of energy deposited by a charged particle per unit path length in the medium through which it is passing. The quality factor is an evaluated fit to the radiobiological efficiency (RBE) of the radiation of a given LET for production of adverse cellular effects. Accuracy in dose equivalent is therefore dependent on the accuracy of particle LET spectra measurements, particularly in the LET region above 3.5 keV/μm where quality factor rises above 1 for charged particles.

A series of passive integrating measurements of the ionizing radiation environment using passive dosimeters located on both the interior and exterior of the Mir Orbital Station was carried out as part of the NASA-Mir Phase 1B Science Program. The Environmental Radiation Measurements on Mir Station experiment consisted of two parts: the Fundamental Biological Investigations 3 (FBI-3) internal experiment and the Fundamental Biological Investigations 4 (FBI-4) external experiment. Objectives of the NASA/Mir Environmental Radiation Measurement Experiment included:

- Measurement of dose rates, dose equivalent rates and LET spectra using passive dosimeters on NASA-2/Mir-21, NASA-3/Mir-22 and NASA-4/Mir-23 missions.
- Mapping of the internal radiation environment of Mir using Area Passive Dosimeters (APDs) located in different Mir modules (Base Block and Kvant 2).
- Determination of the radiation environment external to Mir with measurements of LET spectra and depth dependence of dose on the outer surface of Mir.
- Measurement of the shielding effectiveness of Mir using combined internal and external dosimeters.
- Intercomparison of dose equivalents and LET spectra measured by active (JSC TEPC) and passive (PNTDs, TLDs) dosimeters.
- Intercomparison of measurements made by U.S. and Russian dosimeters.

- Comparison of experimental and calculated dose equivalents and LET spectra for validation of environmental models of trapped and GCR particle spectra and of codes used for propagation of radiation through matter.

To meet these objectives measurements of LET spectra were carried out in the range of 5 to 1250 keV/μm using CR-39 plastic nuclear track detectors (PNTDs) at one location on the external surface of the Mir station and in six area passive dosimeters (APDs) located throughout the interior of the Mir Station. Total absorbed dose was measured using thermoluminescent detectors (TLDs) included inside each APD. Total dose, total dose equivalent and mean quality factor were determined from the combination of absorbed doses and LET spectra measured with the PNTDs. In addition to the USF detectors, each APD contained a detector stack from Institute of Medical and Biomedical Problems (IMBP) in Moscow. APDs were also placed near the NASA JSC Tissue Equivalent Proportional Counter (TEPC) and other active Russian flight dosimeters. Shielding at the three of the four APD locations inside the Mir Base Block have been determined with the aid of a three dimensional mass model. Figures 1 and 2 show the locations of the four APDs in the Base Block and the two APDs in the Kvant 2 module. In addition, Figure 2 shows the location of the External Dosimeter Array (EDA) mounted on the outside of the Kvant 2 module during the NASA-4/Mir-23 and NASA-5/Mir-24 missions.

2. SCIENTIFIC BACKGROUND

2.1 Sources of Ionizing Radiation on the Mir Orbital Station

Astronauts aboard LEO spacecraft like the Mir, Space Shuttle and ISS are exposed to levels of ionizing radiation far in excess of that encountered on the ground. Charged particles in the form of galactic cosmic rays (GCR), trapped protons and electrons, and particles emitted by the sun during solar flares and coronal mass ejections constantly impinge on the outer surface of the spacecraft. The more energetic of these particles penetrate the skin of the spacecraft and interact with the mass of the spacecraft and its contents, producing secondary particles in the process. Secondary particles, especially high energy neutrons, can possess a greater radiobiological effectiveness than the primary particles which produced them. Because of the different types of radiation found in LEO and the broad energy range they occupy, dosimetry aboard spacecraft like Mir and ISS is more challenging than on the ground.

2.1.1 GALACTIC COSMIC RAYS

Galactic cosmic rays (GCR) are charged particles that originate from sources beyond our solar system. The distribution of GCR is thought to be isotropic throughout interstellar space. The energies of GCR particles range from several MeV up to 10^{20} eV and the GCR spectrum peaks around 1 GeV. The GCR spectrum consists of 98% protons and heavier ions (baryon component) and 2% electrons and positrons (lepton component). The baryon component is composed of 87% protons, 12% helium ions (alpha particles) and the remaining 1% heavy ions of charge 3 (Li) through 92 (U). Iron plays a particularly important role in space dosimetry because it is both high in LET and is relatively plentiful compared to other high Z ions [1].

The flux of GCR into our solar system is affected by the sun's eleven year cycle. During that period of the solar cycle called Solar Maximum, when solar activity is most intense, the solar wind attenuates a greater flux of the inbound GCR than during Solar Minimum, when solar activity is least intense. During Solar Minimum the maximum flux of GCR is able to penetrate

into the inner solar system. The NASA/Mir Science Program largely took place during Solar Minimum.

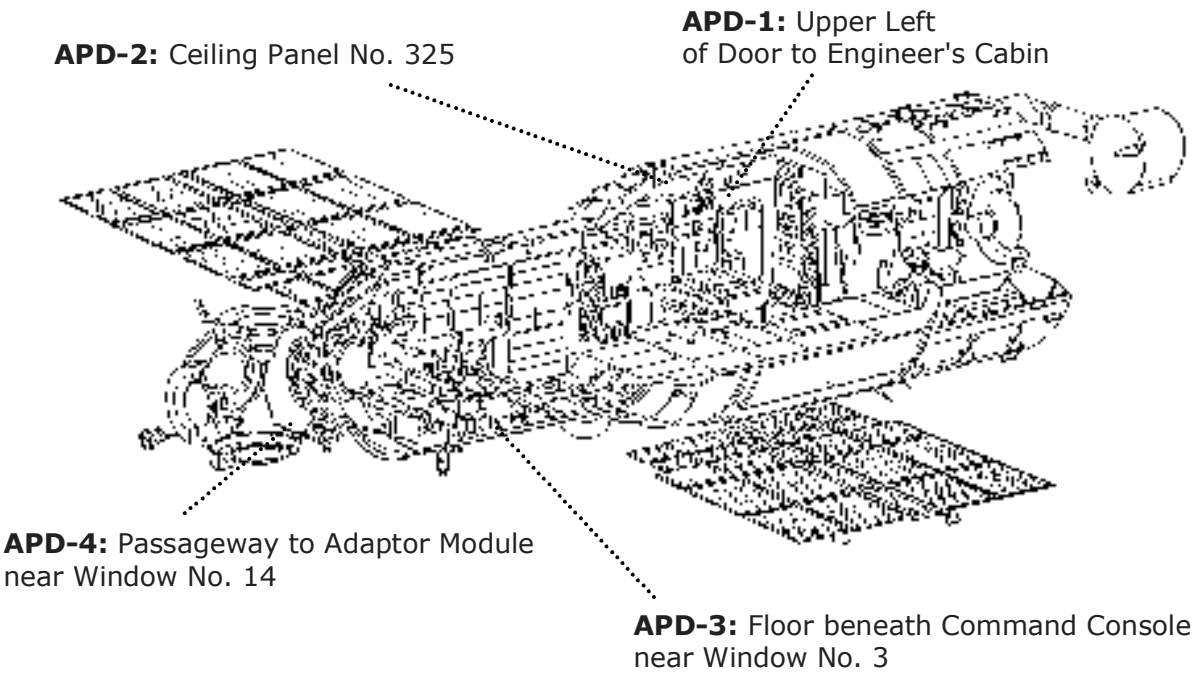

Figure 1. Locations of APD-1, APD-2, APD-3, and APD–4 in the Base Block of the Mir Orbital Station.

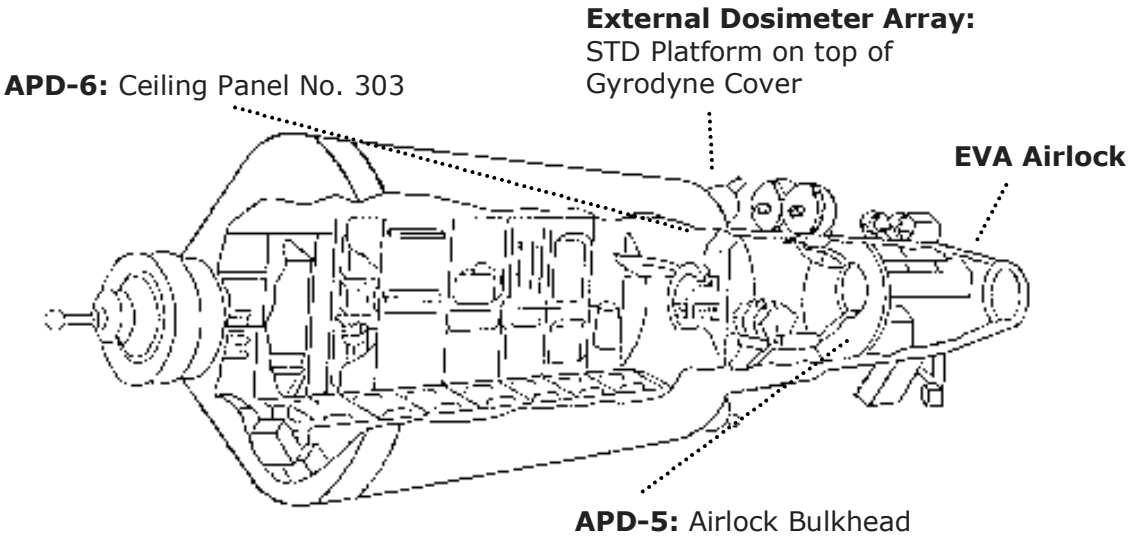

Figure 2. Locations of APD-5 and APD-6 inside the Kvant 2 module, and the External Dosimeter Array on the STD platform mounted on the outer surface of the Kvant 2.

GCR, being composed of charged particles, is also affected by the Earth's magnetic field. Charged particles tend to follow the line of the geomagnetic field. Since the geomagnetic field lines are parallel to the Earth's surface around the equator, all but the most energetic particles are deflected away. The geomagnetic field over the North and South Poles points toward the Earth's surface and GCR particles of all energies are funneled toward the poles at high latitudes. The 51.56° orbit of the Mir is sufficiently highly inclined to receive a substantial exposure from the less energetic GCR[2].

2.1.2 TRAPPED PARTICLES

Surrounding the Earth are intense regions of trapped protons and electrons called the Van Allen Radiation Belts. These particles are trapped by the geomagnetic field where they spiral around the magnetic field lines, bouncing back and forth from mirror points near the poles. The trapped electron spectrum extends in energy from tens of keV to ~5 MeV. Trapped protons extend in energy from several to several hundred MeV and reach a peak between 150 and 250 MeV. Because the electrons are of low energy they are stopped by the shielding provided by the skin of the spacecraft and present little risk to human health. Only the most energetic electrons, interacting with the mass of the station and its contents, will produce Bremstrahlung x-rays[3].

The majority of the trapped proton belt lies at altitudes above that traversed by the orbits of the Mir and ISS. However due to the fact the axis of the Earth's magnetic field is slightly displaced from the Earth's axis of rotation, there is a region off the coast of Brazil called the South Atlantic Anomaly (SAA) where the geomagnetic field drops unusually close to the Earth's surface and the trapped proton belt intersects the orbits of low altitude spacecraft such as the Shuttle, Mir and ISS. When the Mir passes through the SAA, it receives its maximum exposure to trapped protons. For the 51.56° inclination, ~400 km altitude orbit of Mir and ISS, about half the ionizing radiation dose is from trapped protons in the SAA and half is from GCR at higher latitudes [2].

2.1.3 SOLAR PARTICLE EVENTS

The third source of ionizing radiation in LEO is from energetic particles emitted from the sun during solar flares and coronal mass ejections (CME). These solar particle events (SPE) are relatively rare and occur most often during the Solar Maximum phase of the eleven year solar cycle. Most SPEs consist mainly of low energy protons, although higher energy protons and heavy ions can also be emitted. Warning of SPE is often possible ahead of time (a solar flare is seen before the actual particles arrive at the Earth) permitting astronauts and cosmonauts to return inside the spacecraft during EVA and remain in the most heavily shielded portion of the spacecraft until the event is over[4].

Like charged particles from the other space radiation sources, the particles emitted by the sun during an SPE are affected by the Earth's magnetic field. SPE exposure of the Mir only occurred when the spacecraft was near the poles. No major SPEs occurred during the Environmental Radiation Measurements on Mir Station experiment, mainly since it coincided with Solar Minimum. However major SPEs in 1989 and 1991 produced elevated dose levels aboard Mir[5]. The 1991 event produced an enhancement of the trapped particle belts that lasted for several months before finally decaying away.

2.1.4 SECONDARY PARTICLES

As charged particles pass through matter, they interact with the matter in one of two ways– through ionization or through nuclear interactions. Ionization occurs when an incident charged particle interacts with the electrons of the matter through which it passes. These electrons are stripped away from their constituent atoms, leaving the atoms in a highly reactive, ionized state and permitting chemical reactions to occur. A nuclear interaction occurs when a charged particle collides with the nucleus of an atom in the material through which it is passing. Such nuclear interactions can produce secondary particles including neutrons and recoil nuclei. A second source of lower energy neutrons are the albedo neutrons, produced by nuclear interactions of GCR with the nuclei in the Earth's atmosphere. Neutrons are uncharged so they do not interact with matter via ionization. Instead they are very penetrating and readily interact with atomic nuclei via the nuclear strong force.

One way in which ionizing radiation is quantified is in terms of Linear Energy Transfer (LET) spectra. The LET of a particle is a measure of the change in the energy of the particle per unit path length and varies inversely with the energy of the particle. A particle's LET is believed to be of greater relevance than its kinetic energy in terms of radiobiological significance since LET is a measure of energy transferred to the surrounding medium through which the particle is traveling. This transferred energy results in ionization and excitation of the surrounding matter and is responsible for biological damage if the particle is passing through tissue[6]. It is through ionization that the chemical changes in tissue occur that lead to mutations and other stochastic effects. Interactions between secondary neutrons and the nuclei of the surrounding medium often result in high LET particles possessing a large radiobiological effectiveness. Charged secondaries in the form of projectile and target fragments ejected in collisions between charged particles and the nuclei of the spacecraft often possess a higher LET than the original primary particle and consequently also possess a greater radiobiological effectiveness.

3. METHODS/RESEARCH OPERATIONS

Two types of passive radiation detectors were used in the Environmental Radiation Measurements on Mir Station experiment: thermoluminescent detectors (TLD) and CR-39 Plastic Nuclear Track Detectors (PNTDs). The use of TLDs to measure absorbed dose and CR-39 PNTDs to measure LET spectra has become standard on missions of the U. S. Space Shuttle. APDs similar to those deployed aboard Mir during the NASA/Mir Phase-IB Science Program have been included on several Space Shuttle missions since the inception of the program[7]. Similar dosimeters have also been used aboard the NASA Long Duration Exposure Facility (LDEF)[8,9], numerous Russian/Soviet Biocosmos missions and aboard Mir itself during the NASA-1/Mir-18 mission[10].

3.1 Thermoluminescent Detectors

Thermoluminescent detectors or TLDs record the total absorbed dose from ionizing radiation. As a form of passive detector, they accumulate signal over the course of the exposure. This signal is then measured during the readout of the TLD. A TLD is made of solid inorganic crystal. Electrons in the crystal and bound to individual atoms are said to be in the valence band. Electrons shared between the many atoms of the crystal are said to be in the conduction band. As a charged particle passes through the crystal it loses energy by ionizing the atoms of the crystal. Kinetic energy from the charged particle is transferred to electrons in the valence band, elevating

them into the conduction band. In many types of crystal, these electrons in the conduction band readily return to the lower energy state of the valence band and, in doing so, emit photons of visible light. This light can be amplified and its intensity measured using a photomultiplier tube. The amount of light given off as the electrons return from the conduction band to the valence band is directly proportional to the amount of kinetic energy transferred from the charged particle to the valence band electrons in elevating them into the conduction band. In other words, the quantity of visible light measured by the photomultiplier tube is directly proportional to the radiation dose deposited by the charged particle. This is the operating principle behind scintillation-based active radiation detectors. TLDs operate in a similar way, except that when the electrons elevated into the conduction band by the passage of a charged particle try to return to the valence band, they become trapped in sites between the conduction and valence bands called electron traps. These electrons can remain trapped for prolonged periods of time and, as the radiation dose to which the TLD is exposed accumulates, the quantity of trapped electrons correspondingly increases.

When a TLD is heated, a small amount of thermal energy is added to the crystal. This is enough to push the electrons out of their traps and back down to the valence band. As the electrons drop back to the lower energy state of the valence band, they again give off visible light that can be amplified and measured by a photomultiplier tube. The amount of light given off as the TLD is heated is proportional to the radiation dose accumulated by the TLD over the duration of its exposure. Because the TLD only emits light when it is heated, there is no way to know when or for how long the TLD was exposed. Thus it is possible to obtain only dose information averaged over the total exposure time from TLDs. In addition there is no way to tell anything about the total kinetic energy or the charge of the radiation particles. Figure 3 illustrates the how the valence electrons become trapped and are released in TLDs.

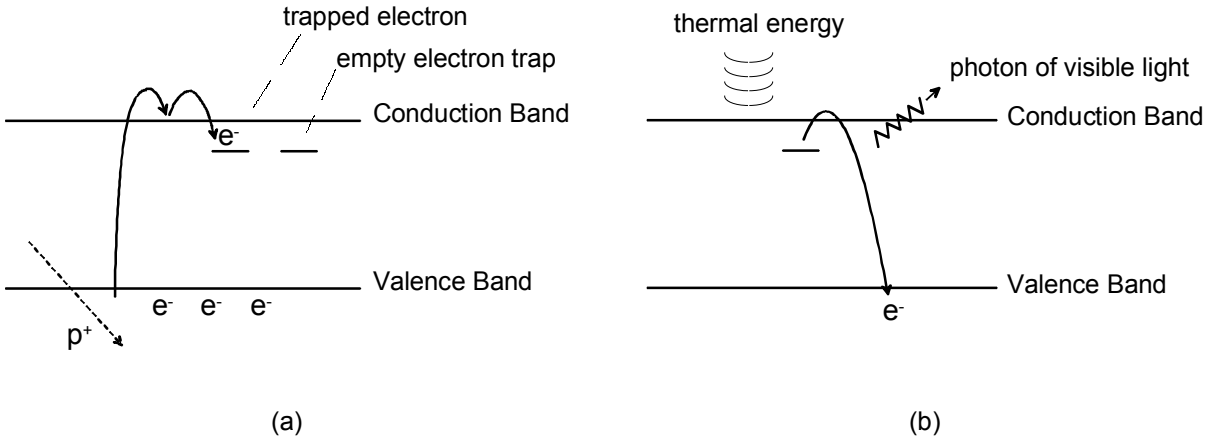

Figure 3. Operation of a TLD. (a) The passage of a charged particle p^+ elevates an electron e^- out of the valence band and into the conduction band. It attempts to drop back into the valence band, but becomes trapped. (b) At time of readout, thermal energy in applied to the TLD, causing the trapped electron to jump out of the trap and fall back to the valence band. As it drops back to the valence band, it releases a photon of visible light that is picked up by the photomultiplier tube.

A TLD reader is an instrument consisting of a light-tight cavity in which to place the TLD, a planchet on which the TLD is heated and a photomultiplier tube to measure the light output from the TLD. By reading out a large number of TLDs exposed to known doses of radiation, the TLD material can be calibrated and a mathematical function relating TLD light output to radiation dose is determined. When a TLD exposed to an unknown radiation dose is read out, its light output is converted to total dose using this function.

Because TLDs do not record any LET information from charged particles, it is not possible to determine Dose Equivalent using TLDs alone. TLDs also record the dose from high-LET particles with decreased efficiency compared to the dose from lower LET particles such x-rays, γ-rays, electrons, and high-energy protons. LET scales as the square of the charge of the radiation particle and heavy ions such as iron nuclei possess LETs several orders of magnitude greater than γ-rays. When a heavy ion traverses a TLD, electron traps immediately surrounding the particle's trajectory quickly become saturated. Thus some of the dose deposited by the heavy ion is not stored as trapped signal and the dose read out from the TLD will be systematically too low. The degree to which the TLD undermeasures the dose from heavy ions is proportional to the LET of the heavy ions. To accurately measure high-LET charged particles and to measure the LET spectrum needed to determine dose equivalent, TLDs are augmented by CR-39 PNTDs.

3.2 CR-39 Plastic Nuclear Track Detectors

CR-39 is a polymer sensitive to charged particles of LET ≥5 keV/μm and comes in the form of thin (~0.6 mm) sheets which are cut to size and then assembled into multi-layer stacks. CR-39 PNTD is directionally sensitive and, to compensate, detector stacks are exposed in three mutually-orthogonal orientations. When passing through a layer of CR-39 PNTD, a charged particle with sufficient LET breaks the molecular bonds of the polymer, forming a path of highly chemically reactive sites along its trajectory. This path of broken chemical bonds is referred to as a latent damage trail. Over the duration of the exposure, as charged particles continually pass through the detector, the latent damage trails in the detector accumulate.

Following exposure, the CR-39 PNTDs are returned to the ground for chemical processing and analysis. The chemical processing of CR-39 PNTD is called etching and consists of soaking the exposed detector layer in a heated bath of strongly alkaline solution, usually sodium hydroxide (NaOH), for an extended period of time. The alkaline solution attacks the surface of the CR-39 layer, dissolving it away at a constant rate. However, the solution attacks the highly reactive sites that make up a latent damage trail at a faster rate. The result is that at the site of the latent damage trail, a conical etch pit is formed in the surface of the detector layer. Figure 4 illustrates the etching process.

After a predetermined length of time, the etching process is halted and the CR-39 layer is removed from the solution and thoroughly rinsed in water. The etch pits, located at the intersections of latent damage trails and the detector surface, are visible as dark cones when viewed through an optical microscope. These conical etch pits are the nuclear tracks. Figure 5 is a photomicrograph of nuclear tracks in a layer of CR-39 PNTD exposed aboard Mir. The size of a nuclear track, when normalized to the quantity of bulk detector material removed during the etching process, is proportional to the LET of the charged particle that produced the original latent damage trail.

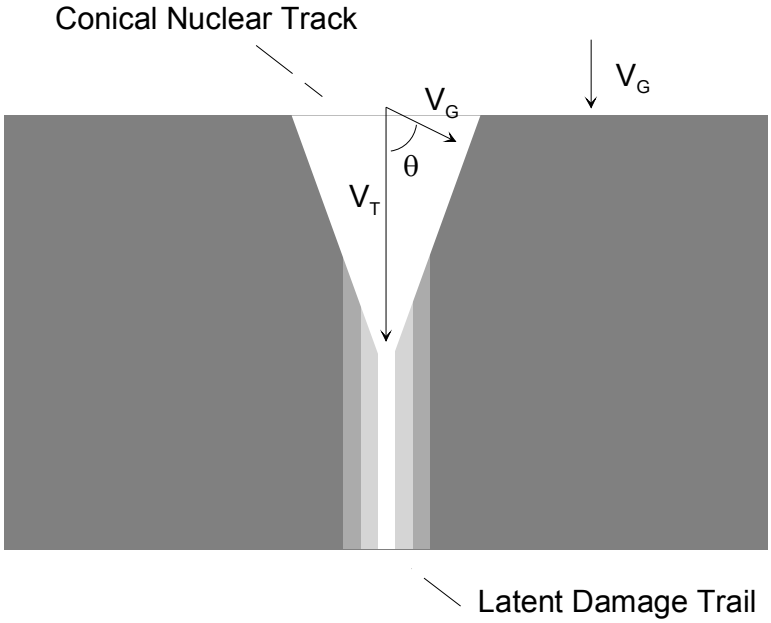

Figure 4. Etching of a Nuclear Track: The alkaline solution attacks the bulk of the CR-39 at a constant rate called the bulk etch rate, V_G. It attacks the latent damage trail at a rate a faster rate, the track etch rate, V_T. The combined action of the two etch rates, V_T and V_G, results in the formation of the conical track.

The calibration of CR-39 PNTDs is largely a matter of relating the size of a track produced by a given etch regimen to the LET of the particle that produced it. Layers of CR-39 are exposed at ground-based particle accelerators to protons and heavy ions of known LET. After a detector layer has been exposed, it is etched and the elliptical openings formed by the intersection of the conical tracks and the detector surface are measured using an optical microscope and micrometer. A large number of such ellipses are measured and the mean track size for that LET is determined. A unitless quantity called the reduced etch rate ratio, V_R, based on the mean track size and the amount of bulk detector material removed during the etching process, is calculated.

Since CR-39 PNTDs exposed in space contain nuclear tracks from charged particles possessing a wide range of LETs, it is the LET fluence spectrum, the number of particles per unit area and solid angle as a function of LET, which is usually measured. The measurement of the LET spectrum in a layer of CR-39 PNTD consists of first measuring all the nuclear tracks within a given area on the detector surface and then calculating the LET of the particles that produced these tracks. A number of corrections to the measured data are then made to compensate for the directional sensitivity of the detector.

A. Functional Objectives

FO1. Measure absorbed doses at six locations inside Mir.
FO2. Measure LET spectra (LET > 5 keV/μm) at six locations inside Mir.
FO3. Combine measurements into total doses and total dose equivalents for six locations inside Mir.
FO4. Measure depth dose at STD platform location outside Mir.
FO5. Measure LET spectra versus depth at STD platform location outside Mir.

B. Hardware Items Used

HWl. TLDs (^{7}LiF- Harshaw TLD-700). 180 of size 1/8 x 1/8 x 0.035 inch. PI-provided.
HW2. CR-39 PNTDs. 238 plates of size 4.5 x 4.5 x 0.06 cm. PI-provided.
HW3. APD boxes (Lexan). 7 boxes of 9.8 x 9.8 x 5.2 cm outer dimensions. PI-provided.
HW4. TLD reader (Harshaw Model 4000). PI-provided.
HW5. PNTD reader (image digitizer system). PI-provided.
HW6. Computers for data reduction and analysis. PI-provided.
HW7. TLDs (^{7}LiF- Harshaw TLD-700). 75 of size 1/8 x 1/8 x 0.0036 inch. PI-provided.
HW8. External Dosimeter Array (EDA) TLD stack holders. NASA-ARC -provided.
HW9. EDA PNTD stack holders. NASA-ARC -provided.

C. Sessions/Functional Objectives (FO) Table

The passive dosimeters (APDs) which were used in this experiment began registering the environmental space radiation from the beginning of NASA-2/Mir-21 through the conclusion of NASA-5/Mir-22 The measurements constituted a single session as described in Table 1 below.

D. Discussion of Method/Protocol

The method for absorbed dose measurements involved:
a. Placing annealed TLDs into two plates at the front and back of each APD.
b. Transporting the 6 APDs on the Shuttle to Mir where they were mounted at different locations.
c. After return the flight TLDs were read out along with calibration and background TLDs.
d. Absorbed doses were generated from the calibration data.

The method for LET spectra measurements involved:
a. Placing 6 stacks of CR-39 plates at the sides of each APD.
b. Transporting the APDs to Mir as in b. above.
c. After return selected CR-39 plates were processed for readout. The processing included etching of the plates in 6.25N NaOH solution at 50° C for either 36 or 168 hr.
d. The processed plates are read out on a semi-automated image digitizer system. For each APD 6 plates are read out; one for each angular orientation in the APD (X, Y, Z) and for each processing time. The parameters measured on each plate are the major and minor diameters of the openings of the particle tracks located within a given area.
e. Track parameter files for the 6 measured plates from an APD, along with the etched thicknesses and the response curves for the CR-39, are used to generate a 4 solid angle averaged LET spectrum for the LET range > 5 keV/,um. The response curves are determined from CR-39 plates irradiated by accelerated particles of known LET. A data base of calibration measurements made in the past at the LBL Bevalac, the German GSI accelerator and several Japanese accelerators are on hand. New calibrations are being performed at the Brookhaven AGS and the Japanese HIMAC heavy ion accelerators.

Table 1. Sessions/Functional Objectives Table

Mission	Session Name	FO#	HW#	Scheduled day	Actual day	Scheduled Subjects	Actual Subjects	Samples/Parameters	Method
NASA-2	Internal space exposure	1,2	1,2,3	Mar. 22, 1996 to Sep. 26, 1996	3/22/96 to 9/26/96	6 flight APDs	6 flight APDs	6 radiation exposures	Passive dosimetry
NASA-3	Internal space exposure	1,2	1,2,3	Sep. 16, 1996 to Jan. 22, 1997	9/16/96 to 1/22/97	6 flight APDs	6 flight APDs	6 radiation exposures	Passive dosimetry
NASA-4	Internal space exposures	1,2	1,2,3	Jan. 12, 1997 to May 24, 1997	1/12/97 to 5/24/97	6 flight APDs	5 flight APDs	5 radiation exposures	Passive dosimetry
NASA-4	External space exposures	4,5	1,2,7, 8,9	April, 1997 to ~ June	4/29/97 to 9/5/97		1 flight EDA 1 flight APD		Passive dosimetry
NASA-5	Return				10/6/97				

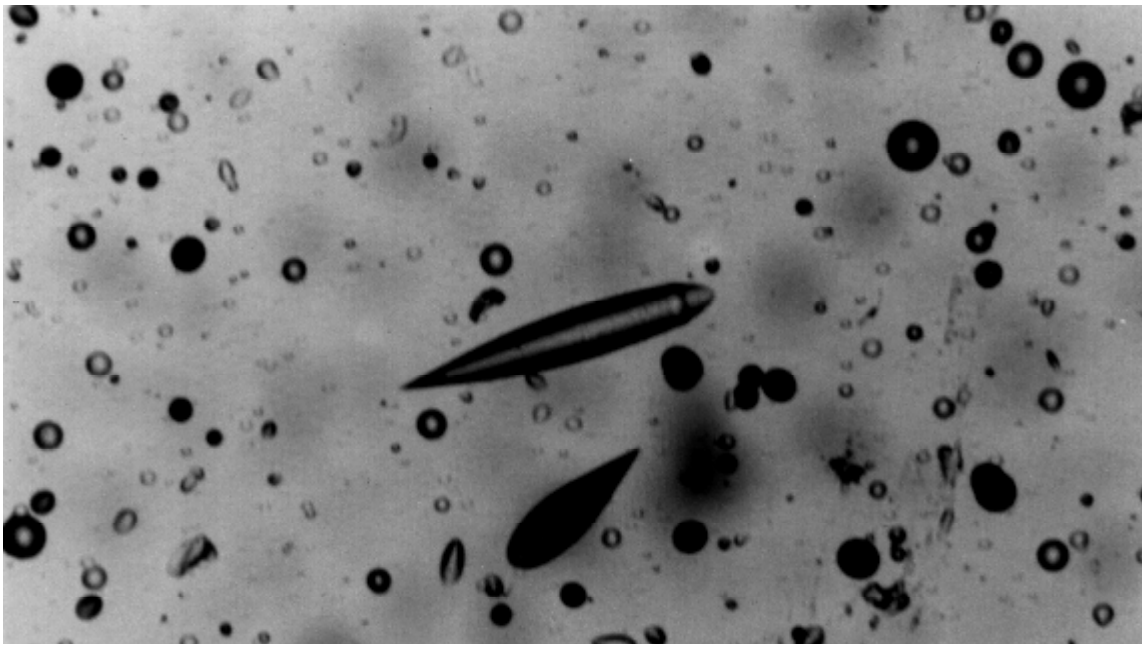

Figure 5. Photomicrograph of tracks in a CR-39 detector exposed during the Environmental Radiation Measurements on Mir Station experiment. The width of the track at the center is ~15 μm.

4. INTERNAL EXPERIMENT

Six Area Passive Dosimeters per mission were deployed throughout the interior of Mir, four inside the Mir Base Block and two inside the Kvant 2 module. The purpose of the APDs was to measure cumulative radiation exposure at different locations inside Mir throughout the mission. Locations of the six APDs are listed in Table 2 and illustrated in Figures 1 and 2.

Table 2. Locations of the APDs inside Mir station.

Detector	Module	Location
APD-1	Base Block	Door to Engineer's Cabin
APD-2	Base Block	Ceiling Panel #325
APD-3	Base Block	Beneath Command Console
APD-4	Base Block	near Window #14
APD-5	Kvant 2	Airlock bulkhead
APD-6	Kvant 2	Ceiling Panel #303

4.1 Area Passive Dosimeter Design

Each APD consisted of polycarbonate box filled with CR-39 plastic nuclear track detectors (PNTDs) and thermoluminescent detectors (TLDs) supplied by University of San Francisco and the IMBP Moscow. The contents of an APD are illustrated in Figure 6 and a fully assembled APD is pictured in Figure 7. Each APD contained six orthogonal stacks of CR-39 PNTD. Each stack possessed four layers of 4.5 cm × 4.5 cm × ~600 μm thick PNTD separated by layers of 8 μm thick Kimfoil polycarbonate foil. Layers of 250 μm thick Lexan polycarbonate were placed on top and bottom of each stack. A stack consisting of 10 layers of 4.5 cm × 4.5 cm × ~600 μm thick CR-39 PNTD was placed at the center of each APD. Two TLD arrays, each measuring 1.7 cm × 4.2 cm and holding ten ^{7}LiF TLDs (TLD-700) were placed in the front and back portions of each APD. An assembled APD measured 9.8 cm × 9.8 cm × 5.5 cm and had a mass of ~0.28 kg. The APDs were attached to the walls and ceiling of the Mir station by means of Velcro. During transfer to and from the Shuttle, the six APDs were stored in a soft stowage pouch.

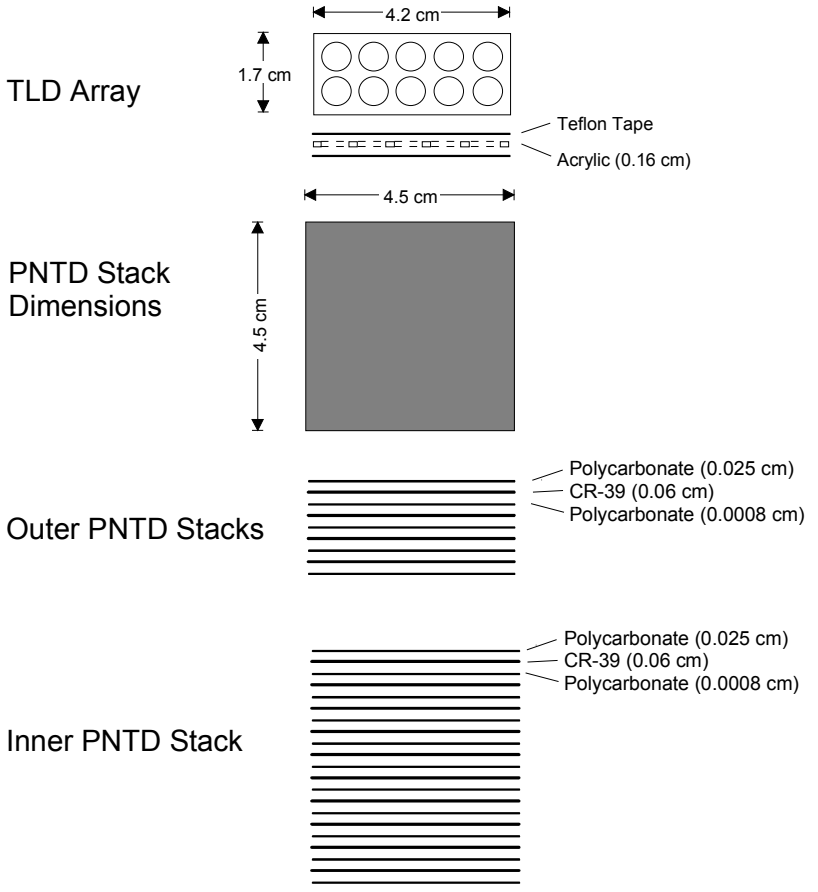

Figure 6. Contents of the Area Passive Dosimeter, not including the passive detector package provided by IMBP, Moscow.

Figure 7. Fully assembled APD in exposure position above door to Flight Engineer's Cabin in the Base Block of the Mir Orbital Station.

4.2 Exposures

Six APDs (Serial Nos. 0001 to 0006) were delivered to Mir aboard STS-76 and deployed in the four locations inside the Base Block and in the two locations inside the Kvant 2 module. Six APDs (Serial Nos. 0007 to 0012) were delivered to Mir aboard STS-79 to replace those delivered on STS-76. One of the six NASA-2 APDs (No. 0005) was inadvertently left aboard Mir while one of the NASA-3 APDs (Serial No. 0010) was returned along with the five NASA-2 APDs. Six NASA-4 APDs (Nos. 0013 to 0018) were delivered to Mir aboard STS-81. APD No. 0005 was returned aboard STS-81 along with Nos. 0007, 0008, 0009, and 0012. NASA-3 APD No. 0011 was inadvertently left aboard Mir during the STS-81 mission while NASA-4 APD No. 0017 was mistakenly returned. APD No. 0018 remained aboard Mir throughout the NASA-4 mission in order to serve as an internal control for the EDA external exposure. Figure 8 shows APD-3 beneath the command console in the Base Block of the Mir Orbital Station.

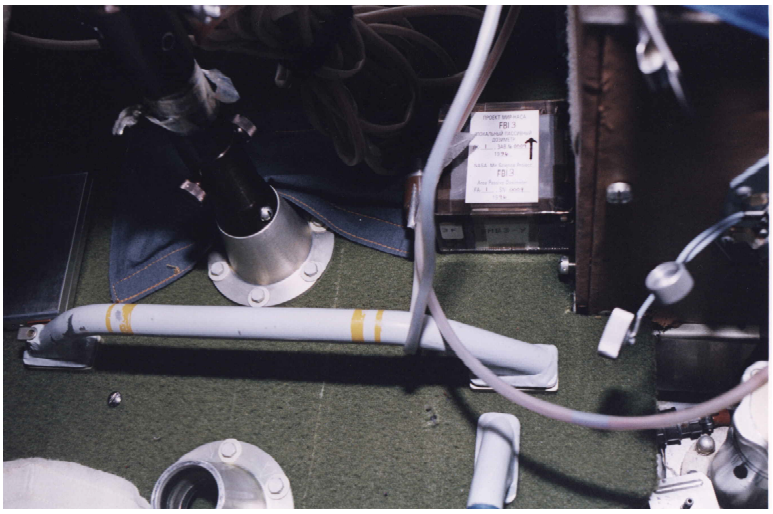

Figure 8. APD-3 on floor beneath the command console, near Window No.3 in the Base Block of the Mir Orbital Station.

4.3 Processing, Readout and Analysis of Internal Experiment

4.3.1 READOUT OF TLDS

Following the return of the APDs to the ground, the APDs from a given mission were disassembled in the Physics Research Laboratory at USF. The TLD arrays were removed from the APD and each TLD was then removed and readout. TLD readout was done using a Harshaw 4000 TLD reader. Ground control TLDs were readout at the same time. Following readout, each TLD was individually calibrated using a standard ^{137}Cs γ-ray source and the TLDs were read out again. Doses for each APD were determined by averaging the individual TLD doses. Mean dose rate was determined by dividing the APD dose by the exposure time.

4.3.2 PROCESSING, READOUT AND ANALYSIS OF CR-39 PNTDS

Two individual layers of CR-39 PNTD from each of three orthogonal stacks in each APD were chemically etched in a solution of 50°C, 6.25 *N* NaOH for periods of 36 hours and 168 hours, respectively. The 36 hour-processed detectors yielded track information for the high-LET, short-range particles (SRP, >~8 μm) including proton-induced target fragment recoils, neutron induced recoils, and primary HZE particles. The 168 hour processed detectors yielded information from long-range particles (LRP, >~40 μm) in the lower LET portion of the spectrum above ≥5 keV/μm. The detectors were read out using a customized version of the ELBEK Automated Track Detector Analysis System. The peak in the differential LET spectrum from relativistic Fe, at 134 keV/μm, was used as an internal calibration. Track data was converted to LET spectra utilizing an empirically derived function relating LET to the measured reduced etch rate ratio, V_R, for each track. The LRP and SRP LET data were combined into a single LET spectrum for each detector orientation. The combined LRP and SRP spectra for each of the three orthogonal detector stacks were then combined into one mean LET spectrum. Figure 9 shows the differential LET flux spectra from the LRP and SRP detectors from APD-1 of the NASA-2/Mir-21

mission. Figure 10 shows the integral LET flux spectra measured in the NASA-2/Mir-21 *x*–, *y*– and *z*–facing detectors and the combined, directionally-independent LET flux spectrum.

In both differential and integral LET spectra, like those shown in Figures 9 and 10, LET is plotted along the *x*–axis. In a differential LET flux spectrum, the number of particles of a given LET on the *x*–axis per cm^2, second, steradian (unit solid angle) is plotted along the *y*–axis. It is essentially a histogram of the particle LETs normalized to the area of detector scanned and the duration of the exposure, and corrected for the directional sensitivity of the detector. In an integral LET flux spectrum, the *y*–axis shows sum of the flux of particles greater than a given LET on the *x*–axis per cm^2, second, steradian. For example for an LET of 100 keV/μm on the *x*–axis of Figure 10, the mean flux as plotted against the *y*–axis shows that there were 2×10^{-5} particles of LET greater than or equal to (≥) 100 keV/μm per cm^2, second, steradian.

4.3.3 DETERMINATION OF DOSE RATE AND DOSE EQUIVALENT RATE

The TLD and PNTD measurements were combined to yield the total dose and dose equivalent rates for the NASA/Mir dosimeters. In this method the low LET (< 5 keV/μm) and high LET (> 5 keV/μm) portions of the dose were separated and a correction was made for the decreased efficiency of high LET particles in TLDs. The efficiency of dose measurement in LiF TLDs as a function of particle LET is given in Figure 11[11]. The fitted curve in the figure is used to find the average dose efficiency of the dose rate spectrum measured by PNTDs in the APD, when measured by the TLDs. The average efficiency is given by:

$$\bar{\varepsilon} = \frac{\sum_{5\ \mathrm{keV}/\mu\mathrm{m}}^{\mathrm{LET}_{max}} \varepsilon(\mathrm{LET})\, D(\mathrm{LET})}{D_{PNTD}}$$

The low LET component of dose is:

$$D_{Low} = D_{TLD} - \bar{\varepsilon}\, D_{PNTD}.$$

The total dose is:

$$D_T = D_{Low} + D_{PNTD}.$$

The total dose equivalent is given by:

$$H_T = D_{Low} + H_{PNTD}.$$

Both D_{PNTD} and H_{PNTD} are calculated directly from the measured LET spectrum. The average quality factor, $\overline{QF}$, of the total measured radiation is then:

$$\overline{QF} = \frac{H_T}{D_T}.$$

Mean dose rate and mean dose equivalent rate were found by dividing dose and dose equivalent, respectively, by the total duration of the exposure.

4.4 Results from the FBI-3 Internal Experiment

4.4.1 ABSORBED DOSE MEASUREMENTS

4.4.1.1 Results from USF TLDs

Absorbed doses as measured by TLDs on the NASA-2/Mir-21, NASA-3/Mir-22 and NASA-4/Mir-23 APDs are given in Tables 3, 4 and 5, respectively. During the NASA-2/Mir-21 mission mean dose rate varied from 268 μGy/d for APD-6 in the Kvant 2 module to 422 μGy/d for APD-3 at the base of the control console in the Base Block or Core module. The average dose rate for each of the five APDs returned by STS-79 was 324 μGy/d. Dose rate for the NASA-3/Mir-22 mission ranged from 265 μGy/d in APD-6 to 378 μGy/d in APD-3. Dose rate for the NASA-4/Mir-22 mission ranged from 273 μGy/d in APD-5 located on the EVA airlock bulkhead in the Kvant-2 module to 361 μGy/d for APD-3. The results illustrate differences in the shielding surrounding the six APD locations with APD-3, in the Base Block (Core) module beneath the command console under the lowest shielding and APD-6 on ceiling panel #303 in the Kvant 2 module being under greatest shielding. The APD-6 location is surrounded by a large amount of equipment and is located immediately beneath the two gyrodynes atop which the EDA was mounted.

The second observation seen in the TLD absorbed dose rates is that the dose rates decreased for each of the successive NASA/Mir mission. The most likely reason for this decrease was the decrease in altitude of the Mir Station over this period. Dose rate scales exponentially with altitude in the South Atlantic Anomaly. Due to atmospheric drag, the Mir continually loses altitude and must periodically be reboosted to a higher altitude.

Table 3. Absorbed doses and mean dose rates measured by USF TLDs during the NASA-2/Mir-21 mission (3/22/96 – 9/26/96, 188.2 days).

APD	APD Serial No.	TLD Plate	Absorbed Dose (mGy)	Mean Dose Rate (μGy/d)
NMA-1	0001	Front	60.9 ± 1.8	324 ± 10
		Back	62.5 ± 1.9	332 ± 10
NMA-2	0002	Front	54.5 ± 1.6	290 ± 9
		Back	53.9 ± 1.6	286 ± 9
NMA-3	0003	Front	79.4 ± 2.4	422 ± 13
		Back	73.7 ± 2.2	392 ± 12
NMA-4	0004	Front	59.7 ± 1.8	317 ± 10
		Back	61.9 ± 1.9	330 ± 10
NMA-6	0006	Front	50.5 ± 1.5	268 ± 8
		Back	51.7 ± 1.6	275 ± 9
NMB-4*	0010	Front	3.12 ± 0.09	308 ± 9
		Back	3.35 ± 0.10	330 ± 10

*Only exposed for 10.138 days

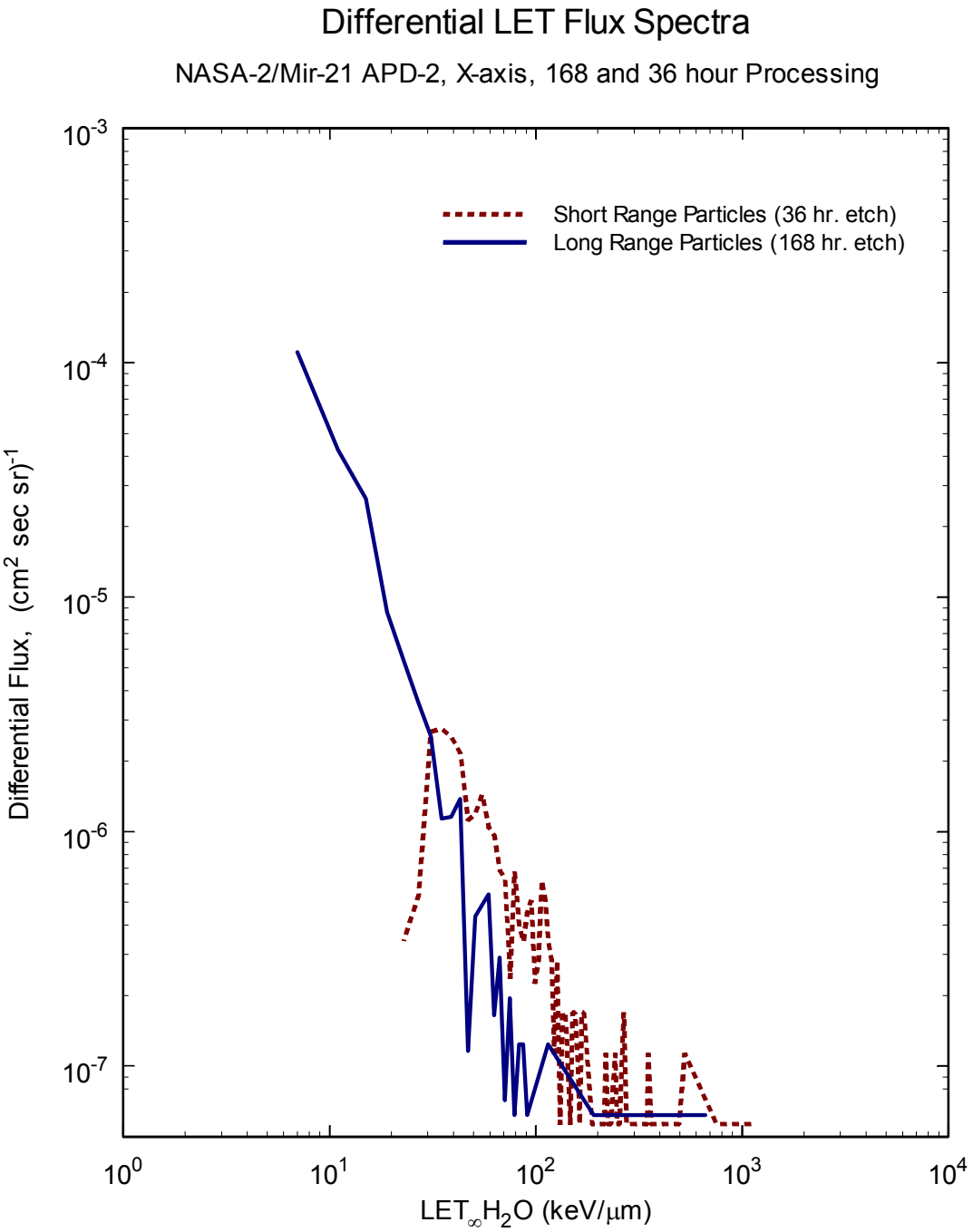

Figure 9. The differential LET flux spectrum measured in the SRP (36 hour etch) and LRP (168 hour etch) *x*–axis detectors from APD-1 exposed on the NASA-2/Mir-21 mission.

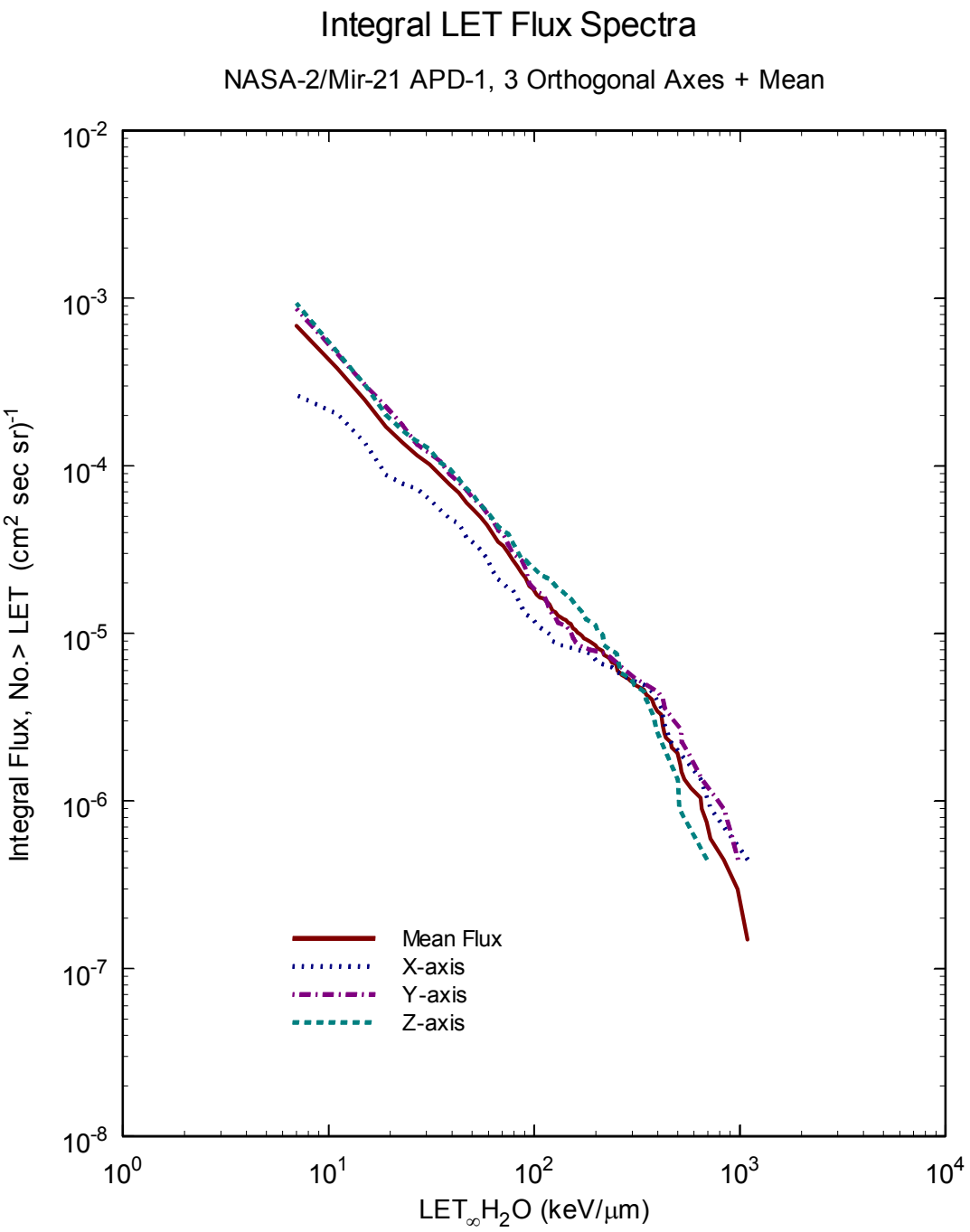

Figure 10. Integral LET flux spectra from the *x*–, *y*–, and *z*–axis detectors and the resulting 4π averaged LET flux spectrum from APD-1 exposed on the NASA-2/Mir-21 mission.

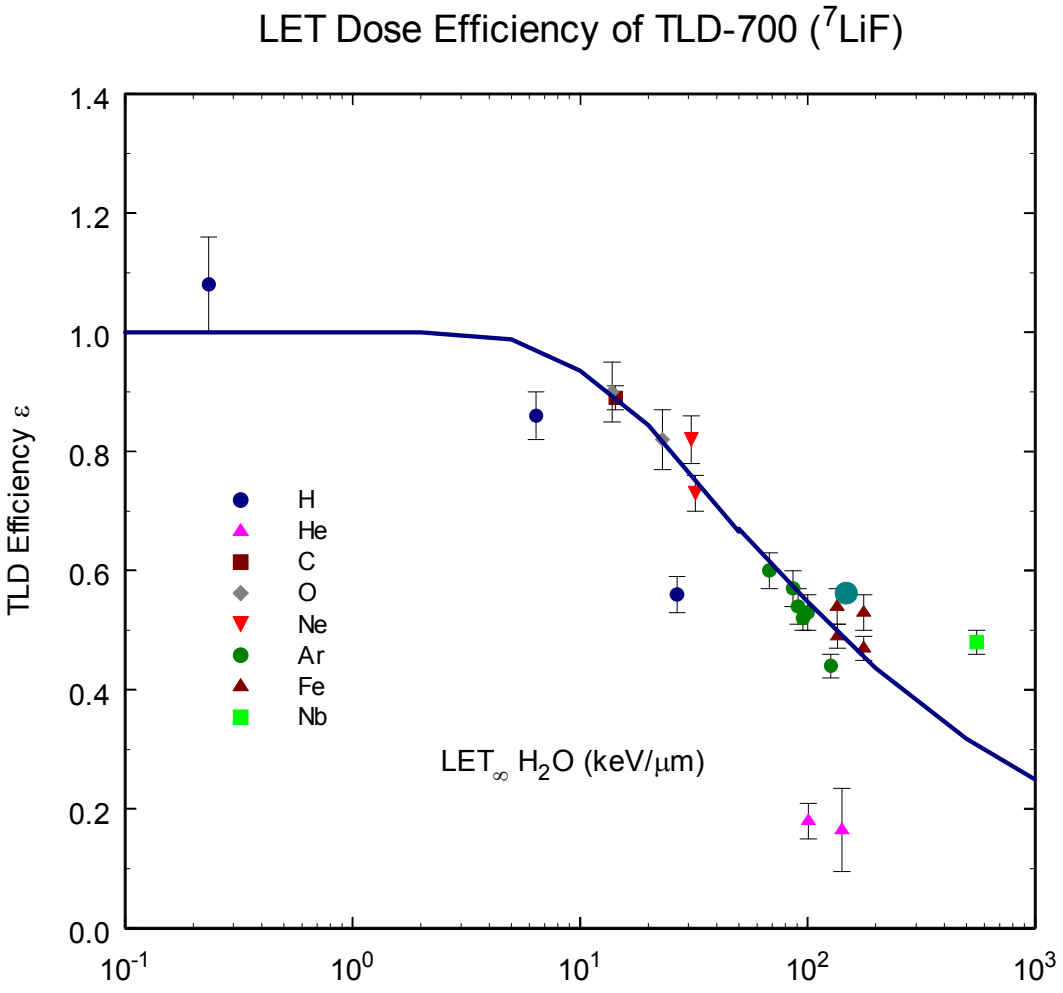

Figure 11. TLD dose registration efficiency as a function of LET. The empirically fit equation is used to correct the Dose as measured by TLD for high LET particles[11].

Table 5. Absorbed doses and mean dose rates measured by USF TLDs during the NASA-3/Mir-22 mission (9/16/96 – 1/22/97, 127.2 days).

APD	APD Serial No.	TLD Plate	Absorbed Dose (mGy)	Mean Dose Rate (μGy/d)
NMB-1	0007	Front	39.0 ± 1.2	306 ± 9
		Back	39.6 ± 1.2	311 ± 9
NMB-2	0008	Front	34.6 ± 1.0	272 ± 8
		Back	34.9 ± 1.0	274 ± 8
NMB-3	0009	Front	49.9 ± 1.5	392 ± 12
		Back	46.5 ± 1.4	365 ± 11
NMB-6	0012	Front	33.2 ± 1.0	269 ± 8
		Back	61.9 ± 1.9	261 ± 8
NMA-5*	0005	Front	128.1 ± 3.8	420 ± 12
		Back	129.1 ± 3.9	423 ± 13
NMC-5**	0017	Front	2.46 ± 0.07	241 ± 7
		Back	2.49 ± 0.07	244 ± 7

*Exposed during both NASA-2/Mir-21 and NASA-3/Mir-22 missions for a total duration of 305.26 days.
**Exposed for only 10.206 days.

Table 6. Absorbed doses and mean dose rates measured by USF TLDs during the NASA-4/Mir-23 mission (1/12/97 – 5/24/97, 132.1 days).

APD	APD Serial No.	TLD Plate	Absorbed Dose (mGy)	Mean Dose Rate (μGy/d)
NMC-1	0013	Front	41.6 ± 1.2	320 ± 9
		Back	42.4 ± 1.3	326 ± 10
NMC-2	0014	Front	34.6 ± 1.0	272 ± 8
		Back	34.9 ± 1.0	274 ± 8
NMC-3	0015	Front	48.7 ± 1.5	374 ± 12
		Back	45.2 ± 1.4	347 ± 11
NMC-4	0016	Front	39.3 ± 1.2	302 ± 9
		Back	38.9 ± 1.2	299 ± 9
NMB-5*	0011	Front	66.3 ± 2.0	268 ± 8
		Back	68.8 ± 2.1	278 ± 8
NMC-6**	0018	Front	75.6 ± 2.3	283 ± 9
		Back	76.9 ± 2.3	288 ± 9

*Exposed during both NASA-3/Mir-22 and NASA-4/Mir-23 missions for a total duration of 249.37 days.
**Exposed during both the NASA-4/Mir-23 and NASA-5/Mir-24 missions for a total duration of 267.47 days.

4.4.1.2 Comparison with IMBP Results

Independent measurements of absorbed dose using TLDs were carried out by IMBP in the six APDs. Data is only available for the IMBP dose measurements made during the NASA-2/Mir-21 mission. Table 7 shows a comparison of absorbed dose and mean dose rate as measured by TLD-700 by USF and by TLD-600 and TLD-700 by IMBP. TLD-600 is ^{6}LiF and, in addition to being sensitive to low LET radiation like TLD-700 (^{7}LiF), it possesses an enhanced sensitivity to low energy neutrons (<1 MeV) via the ^{6}Li(n,^{3}H)α reaction. By comparing doses measured by TLD-600 with TLD-700, and by using appropriate calibration functions, one can estimate the low energy neutron contribution to dose. For Mir, the low energy neutron contribution was expected to be extremely small, as borne out in the IMBP measurements. The IMBP measurements are systematically higher than those of USF. At present, the reason for this is not known. It is possible that the IMBP TLDs were subjected to higher background exposure prior to and following to flight aboard Mir, since the IMBP detector packages had to be transported to and from the US for inclusion in the USF APDs.

Table 7. Comparison of absorbed doses and mean dose rates as measured by USF and IMBP in the six APDs during the NASA-2/Mir-21 mission.

Detector	Location	Quantity	USF Results	IMBP Results	
				TLD-700	TLD-600
APD-1	Core Module	Dose	67.1 ± 1.9 mGy	74.2 ± 2.1 mGy	75.7 ± 1.9 mGy
	Door to Engineer's Cabin	Dose Rate	328 ± 10 μGy/d	396 ± 11 μGy/d	402 ± 10 μGy/d
APD-2	Core Module	Dose	54.2 ± 1.6 mGy	65.3 ± 0.8 mGy	68.7 ± 2.3 mGy
	Ceiling Panel #325	Dose Rate	288 ± 9 μGy/d	347 ± 4 μGy/d	365 ± 12 μGy/d
APD-3	Core Module, beneath	Dose	76.6 ± 2.4 mGy	93.2 ± 1.7 mGy	91.1 1.5 mGy
	Command Console	Dose Rate	407 ± 13 μGy/d	495 ± 9 μGy/d	484 ± 8 μGy/d
APD-4	Adaptor Module	Dose	60.8 ± 1.9 mGy	67.9 ± 1.3 mGy	70.2 ± 1.3 mGy
	near Window #14.	Dose Rate	324 ± 10 μGy/d	361 ± 7 μGy/d	373 ± 7 μGy/d
APD-6	Kvant 2	Dose	51.1 ± 1.6 mGy	58.5 ± 1.1 mGy	60.0 ± 0.9 mGy
	Ceiling Panel #303	Dose Rate	271 ± 9 μGy/d	311 ± 6 μGy/d	319 ± 5 μGy/d

4.4.1.3 Comparison with other TLD Dose Measurements

TLDs were also exposed for purposes of absorbed dose measurement by other research groups near two of the APD locations prior to and simultaneous with exposure of the USF APDs. USF exposed a single APD during the NASA-1/Mir-18 mission at the APD-2 location on Ceiling Panel 325. NASA Johnson Space Center exposed an array of TLD-100 (natural LiF) during the NASA-2/Mir-21 and NASA-3/Mir-22 missions. NASA-JSC also exposed TLD arrays near Window No. 14, the APD-4 location, in the adaptor module during NASA-2/Mir-21 and NASA-3/Mir-22 [12]. The Institute of Space Dosimetry (ISDA), Vienna, Austria, has carried out a number of experiments aboard the Mir to measure absorbed dose, including during the Mir-19 mission in 1995[13]. A comparison of TLD absorbed dose measurements made at the APD-2 location is presented in Table 8 while a comparison of TLD absorbed dose measurements made at the APD-4 location in the adaptor module, near Window No. 14, is presented in Table 9.

Differences between dose rates made at different times most likely reflect differences in altitude. Less easily explained are differences in dose rates measured at the same time. Most notable is the fact that

during the NASA-2/Mir-21 and NASA-3/Mir-22 missions, dose rates measured by the NASA-JSC TLDs were systematically higher than those measured by USF. Some of the difference may be due to subtle differences in the shielding of the two detectors. However it is unlikely that this can explain the difference in its entirety. It is possible that differences in technique and/or ground-based calibration of the TLDs may be responsible.

Table 8. Absorbed dose measurements made using TLDs at the APD-2 location on Ceiling Panel No. 325 near R-16 Operational Dosimeter, mean shielding = 44 g/cm^2[12,13].

Experiment/ Institution	Exposure Dates	Duration (days)	Dose (mGy)	Dose Rate (μGy/d)
Mir-18/USF	2/28/95-7/7/95	129	34.0 ± 0.7	264 ± 5
Mir-19/ISDA TLD-600	6/27/95-11/20/95	145	59.7 ± 1.6	427 ± 10
Mir-19/ISDA TLD-700	6/27/95-11/20/95	145	55.1 ± 1.1	410 ± 32
NASA-2/USF	3/22/96-9/26/96	188.2	54.2 ± 1.6	288 ± 9
NASA-2/IMBP TLD-600	3/22/96-9/26/96	188.2	65.3 ± 0.8	347 ± 4
NASA-2/IMBP TLD-700	3/22/96-9/26/96	188.2	68.7 ± 2.3	365 ± 12
NASA-2/JSC	3/22/96-9/26/96	188.2	74.1 ± 0.8	394 ± 4
NASA-3/USF	9/16/96-1/22/97	127.2	34.8 ± 1.0	273 ± 8
NASA-3/JSC	9/16/96-1/22/97	127.2	44.2 ± 0.5	346 ± 3
NASA-4/USF	1/12/97-5/24/97	132.1	37.3 ± 1.1	287 ± 8

Table 9. APD-4: Adaptor module, near Window #14, 38 g/cm^2[12,13].

Experiment/ Institution	Exposure Dates	Duration (days)	Dose (mGy)	Dose Rate (μGy/d)
Mir-19/ISDA TLD-600	6/27/95-11/20/95	145	52.4 ± 0.9	361 ± 6
Mir-19/ISDA TLD-700	6/27/95-11/20/95	145	51.3 ± 2.0	354 ± 14
NASA-2/USF	3/22/96-9/26/96	188.2	60.8 ± 1.9	324 ± 10
NASA-2/IMBP TLD-600	3/22/96-9/26/96	188.2	67.9 ± 1.3	361 ± 7
NASA-2/IMBP TLD-700	3/22/96-9/26/96	188.2	70.2 ± 1.3	373 ± 7
NASA-3/JSC	9/16/96-1/22/97	127.2	42.0 ± 0.8	327.8 ± 4
NASA-4/USF	1/12/97-5/24/97	132.1	39.1 ± 1.2	300 ± 9

4.4.2 LET SPECTRA MEASUREMENTS IN CR-39 PNTD

4.4.2.1 Integral LET Spectrum Measurements

Integral LET flux, dose rate, and dose equivalent rate spectra have been generated from measurements of the APD CR-39 PNTDs. Figures 12, 13, and 14 show the integral LET flux, dose rate, and dose equivalent rate spectra measured on the NASA-2/Mir-21 mission, respectively. Figures 15, 16, and 17 show the integral LET flux, dose rate, and dose equivalent rate spectra, respectively, measured from the NASA-3/Mir-22 APDs. Figures 18, 19, and 20, respectively, show the integral LET flux, dose rate and dose equivalent rate spectra measured during the NASA-4/Mir-23 mission.

In Figure 12, the integral LET flux spectra measured for the five APDs included in the NASA-2/Mir-21

missions, there is close agreement between the five curves throughout the entire measured range from 5 to 1250 keV/μm. The curve from APD-6 lies somewhat below the others for LET ≥ 100 keV/μm. This is consistent with the lower dose rate measured in the APD-6 TLDs. The high LET region (≥ 100 keV/μm) is primarily made up of short-range (~8 μm) secondary particles produced in target fragmentation events when primary protons interact with the C and O nuclei of the detector. Greater shielding at the APD-6 location is seen as both a decrease in total dose and a decrease in the relative number of target fragment events. Most of the curves are seen to change slope between 250 and 350 keV/μm. This knee occurs at the approximate maximum LET for α-particles (~230 keV/μm). Below this knee, most of the LET spectra is believed to be made up of knockout protons and α-particles produced in target fragmentation events and from proton recoils produced in interactions with secondary neutrons. The spectrum above ~300 keV/μm is the result of GCR and the heavier target fragments. The lower rate of production of these heavier fragments relative to protons and α-particles is most likely the cause of the steepening slope above ~300 keV/μm.

Mean dose rate spectra for the NASA-2/Mir-21 APDs were generated from the averaged flux results and are shown in Figure 13. Dose equivalent rate spectra were calculated using the ICRP-26 quality factors and the results are presented in Figure 14. As seen in the LET flux spectrum, there is good agreement between all the dose rate and dose equivalent rate curves, though the spectrum measured for APD-6 falls somewhat below the others. As stated earlier, this is most likely due to the APD-6 location in the Kvant 2 module being more heavily shielded than the other four locations in the Core or Base Block module.

The integral LET flux measurements made in CR-39 PNTDs exposed during the NASA-3/Mir-22 mission, shown in Figure 15, are similar to those measured in the NASA-2/Mir-21 mission (Figure 12). There is fairly close agreement amongst the four spectra measured, except at high LETs (≥100 keV/μm). In the high LET region, APD-2 lies below the other curves, while APD-6 in the Kvant 2, is the highest. The most likely reason for this difference is a change in the shielding environments surrounding those locations. Another possible explanation is a change in the orientation of the station during the NASA-3/Mir-22 mission. Figure 16, the integral LET dose rate spectra, measured in the NASA-3/Mir-22 APDs show a similar trend. Over most of the measured range, APD-6 in the Kvant 2 module has the highest dose rate while APD-2, on Ceiling Panel 325 in the Base Block is the lowest. However, at the higher LET, above ~700 keV/μm, the APD-6 dose rate spectrum falls below that of APD-2. This feature is even more prominent in Figure 17, the dose equivalent rate spectra for the NASA-3/Mir-22 mission. Here the spectrum measured in APD-6 is the lowest. While APD-6 received the highest flux of low LET particles and thus had the highest flux spectrum, it received the smallest contribution for high LET particles and thus received a correspondingly lower dose equivalent.

As with the NASA-2/Mir-21 and NASA-3/Mir-22 LET flux spectra, the integral LET flux spectra measured on the NASA-4/Mir-23 mission, Figure 18, are in fairly close agreement throughout most of the measured range. Only at LET ≥100 keV/μm is there much variation. Here APD-3, near the Window No. 3 beneath the command console in the Base Block received the lowest high-LET contribution, while APD-2 had the highest. This result is further reflected in the dose rate spectra, Figure 19, and the dose equivalent rate spectra, Figure 20. As with the previous mission, the most likely explanation for this difference lies in changes in the shielding environment immediately surrounding the detectors and/or in a reorientation of the station.

Figure 21 shows the integral LET flux spectra measured for APD-1 during the NASA-2/Mir-21 mission between 22 March and 26 September 1996, the NASA-3/Mir-22 mission between 16 September 1996 and 22 January 1997 and the NASA-4/Mir-23 mission between 12 January and 22 May 1997. APD-1 was located at the entrance to the Flight Engineer's sleeping quarters in the large diameter portion of the Mir Core Module. The spectra during the first two missions are in agreement within the limits of

uncertainty of the measurement over the entire LET range measured, indicating that little change in the LET spectra above 5 keV/μm occurs over such short time scales. However the spectrum measured for the NASA-4/Mir-23 mission lies substantially above the other two, especially at high LET (≥100 keV/μm). This increase in the high LET portion of the spectrum probably reflects a larger number of proton and neutron induced target fragments. A similar increase in the spectrum during the NASA-4/Mir-23 mission as compared to the two earlier missions can also be seen in a comparison of the integral LET flux spectra measured at the APD-2 location, as shown in Figure 22. APD-2 was positioned near the R-16 operational dosimeter, on Ceiling Panel No. 325 in the Base Block of the Mir.

3.4.2.2 Comparison of USF PNTD And JSC-TEPC LET Spectra

A comparison of the NASA-2/Mir-21 integral Lineal Energy Transfer flux spectrum measured by the NASA Johnson Space Center Tissue Equivalent Proportional Counter (JSC-TEPC) with the PNTD results is shown in Figure 23[12]. The two spectra for both types of detector are comparable over almost the entire LET range shown. The deviation of the results below about 20 keV/μm is due to a fall off in the detection efficiency of the PNTDs. Differences above about 100 keV/μm are expected due to the differing chemical compositions of the two types of detector media. Above 100 keV/μm, most of the spectrum is produced by proton-induced, short-range, high-LET target fragments. Target fragment production is dependent on the elemental composition of the medium through with the primary protons pass. The greater concentration of C and O nuclei per unit volume in the CR-39 PNTDs versus the sensitive volume of the TEPC leads to the higher signal in the LET region above 100 keV/μm.

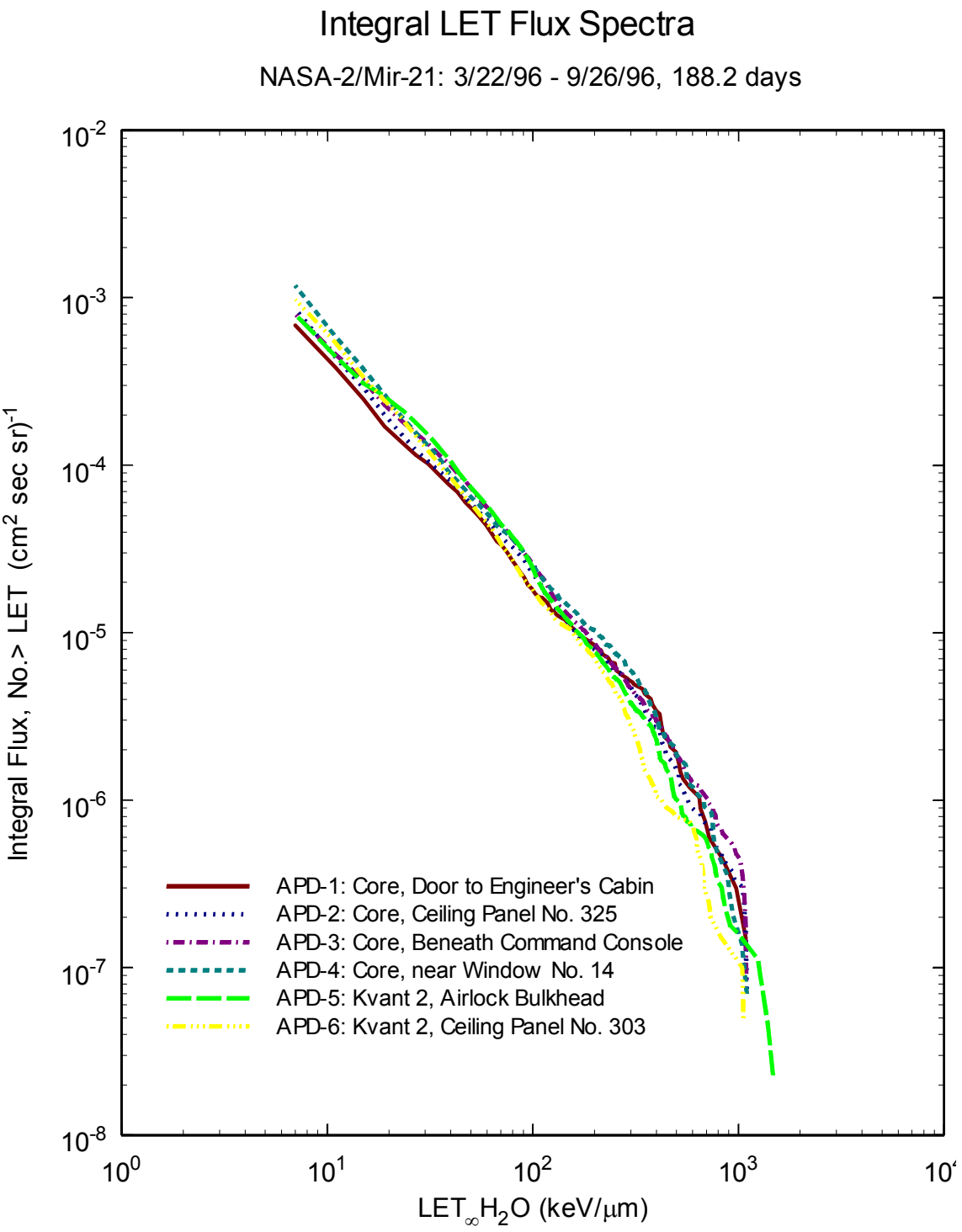

Figure 12. Integral LET flux spectra measured inside the Mir Orbital Station during the NASA-2/Mir-21 mission by the Environmental Radiation Measurements Experiment. 22 March – 26 September 1996. APD-5 was exposed for 305.3 days on both the NASA-2/Mir-21 and NASA-3/Mir-22 missions.

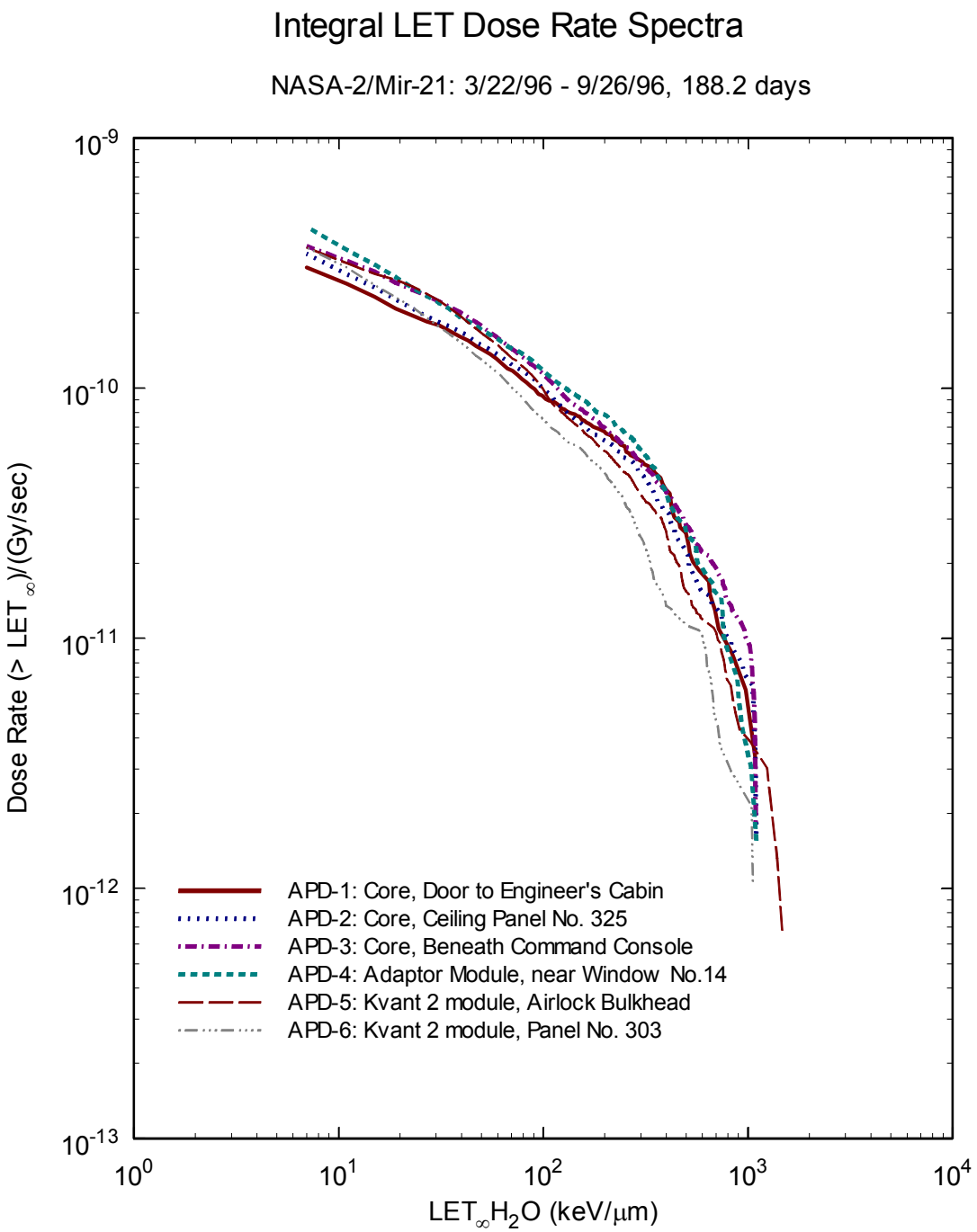

Figure 13. Integral LET dose rate spectra measured inside the Mir Orbital Station during the NASA-2/Mir-21 mission by the Environmental Radiation Measurements Experiment. 22 March – 26 September 1996. APD-5 was exposed for 305.3 days on both the NASA-2/Mir-21 and NASA-3/Mir-22 missions.

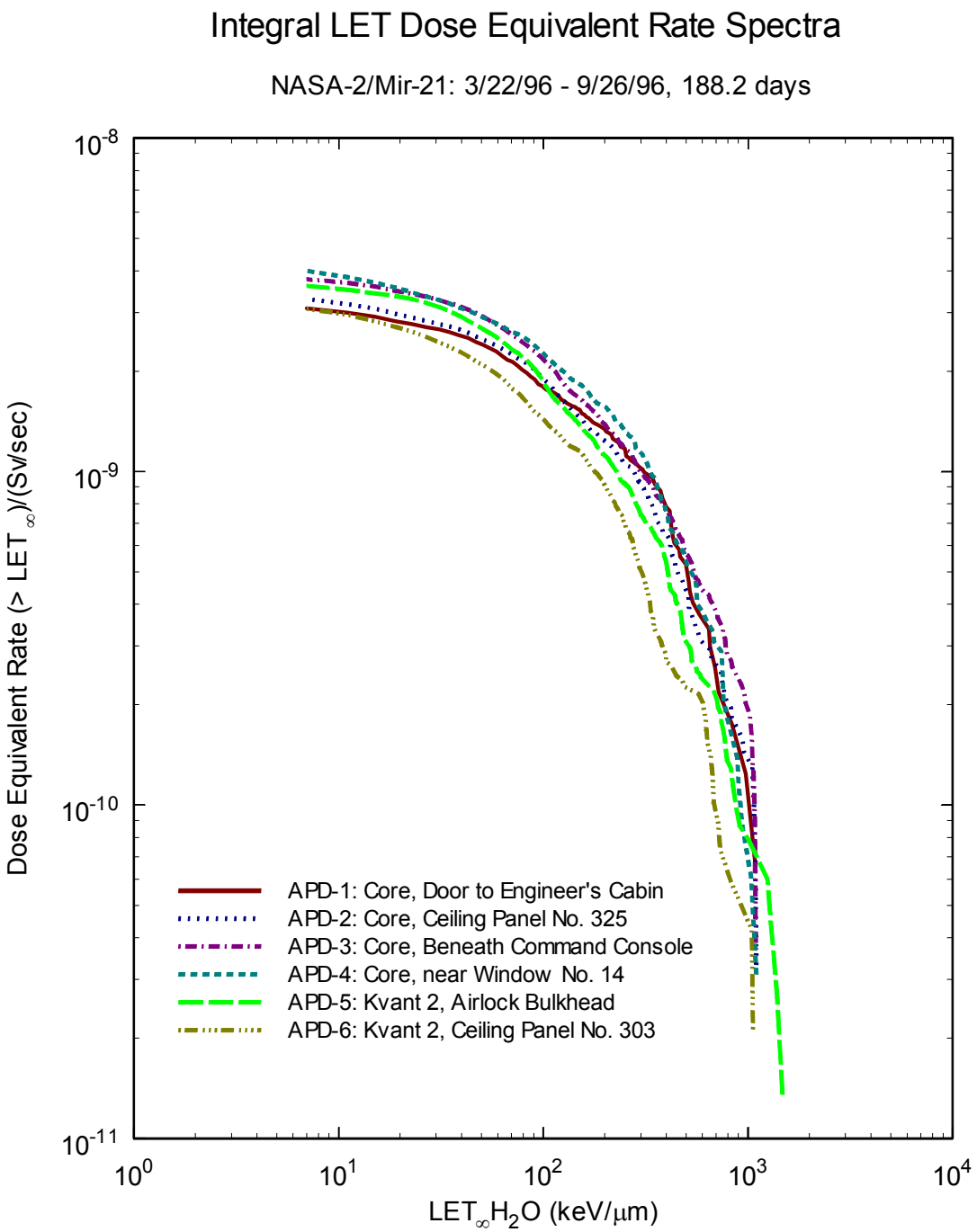

Figure 14. Integral LET dose equivalent rate spectra measured inside the Mir Orbital Station during the NASA-2/Mir-21 mission by the Environmental Radiation Measurements Experiment: 22 March 1996–26 September 1996. APD-5 was exposed for 305.3 days on both the NASA-2/Mir-21 and NASA-3/Mir-22 missions.

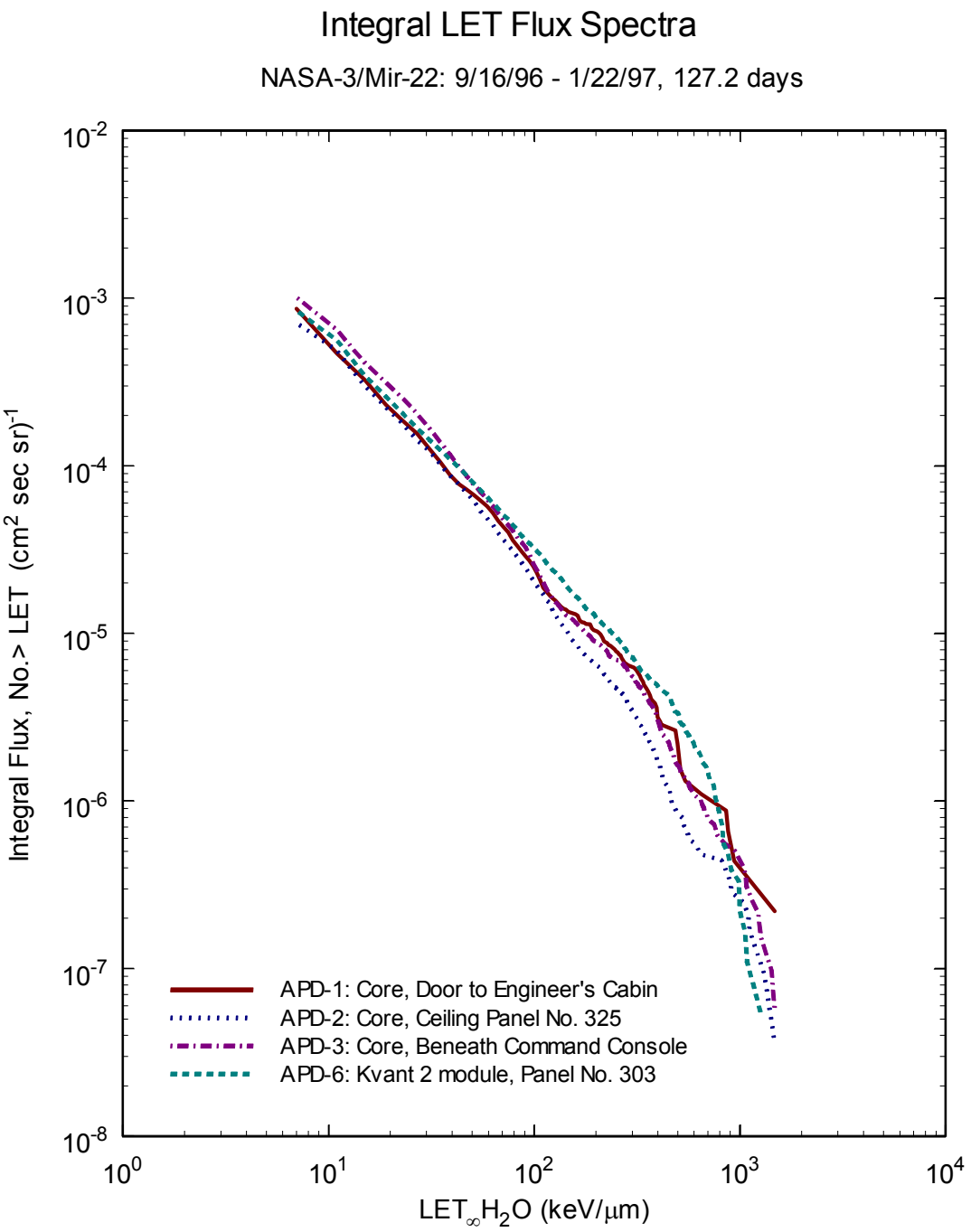

Figure 15. Integral LET flux spectra measured inside the Mir Orbital Station during the NASA-3/Mir-22 mission by the Environmental Radiation Measurements Experiment: 16 September 1996–22 January 1997.

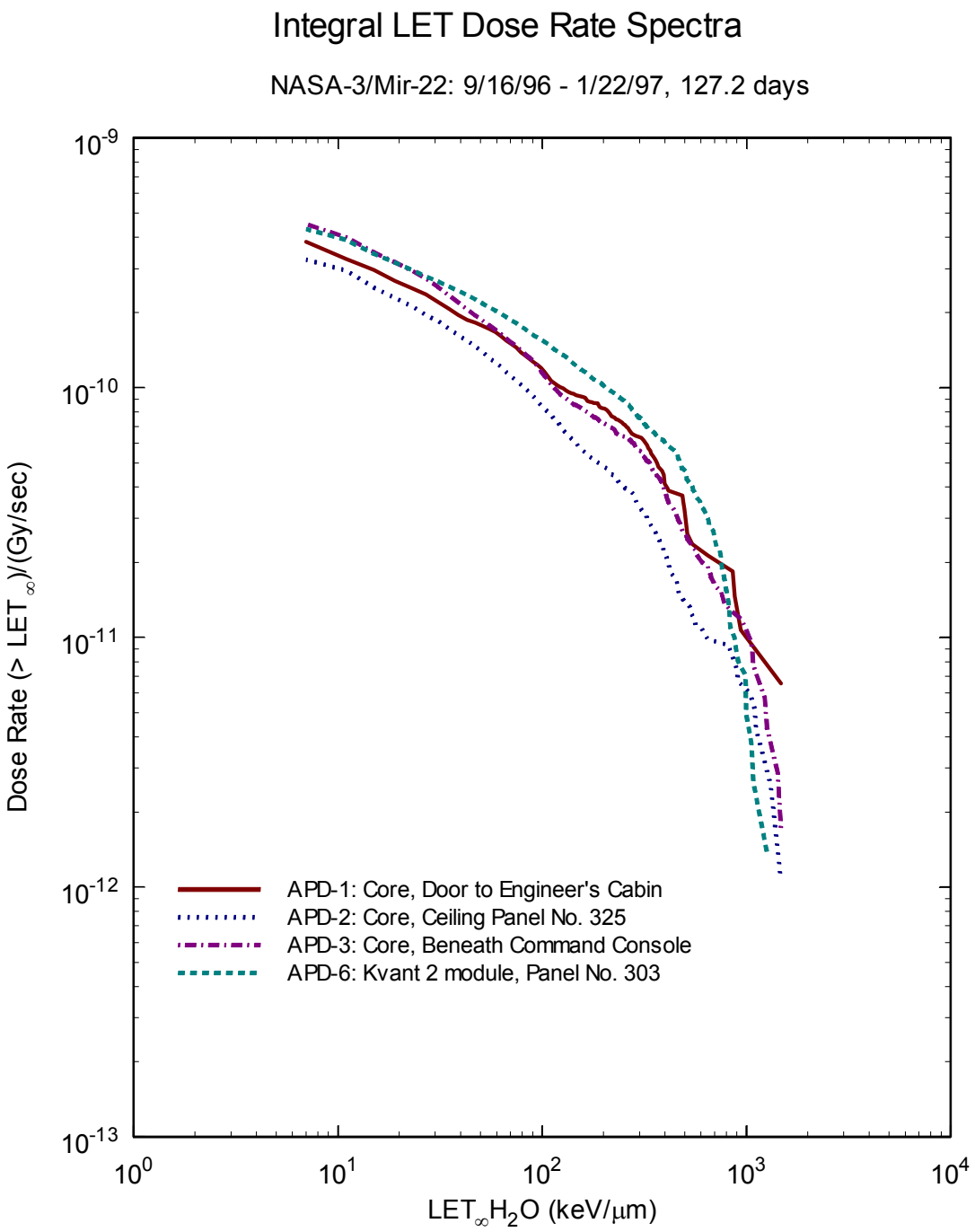

Figure 16. Integral LET dose rate spectra measured inside the Mir Orbital Station during the NASA-3/Mir-22 mission by the Environmental Radiation Measurements Experiment: 16 September 1996–22 January 1997.

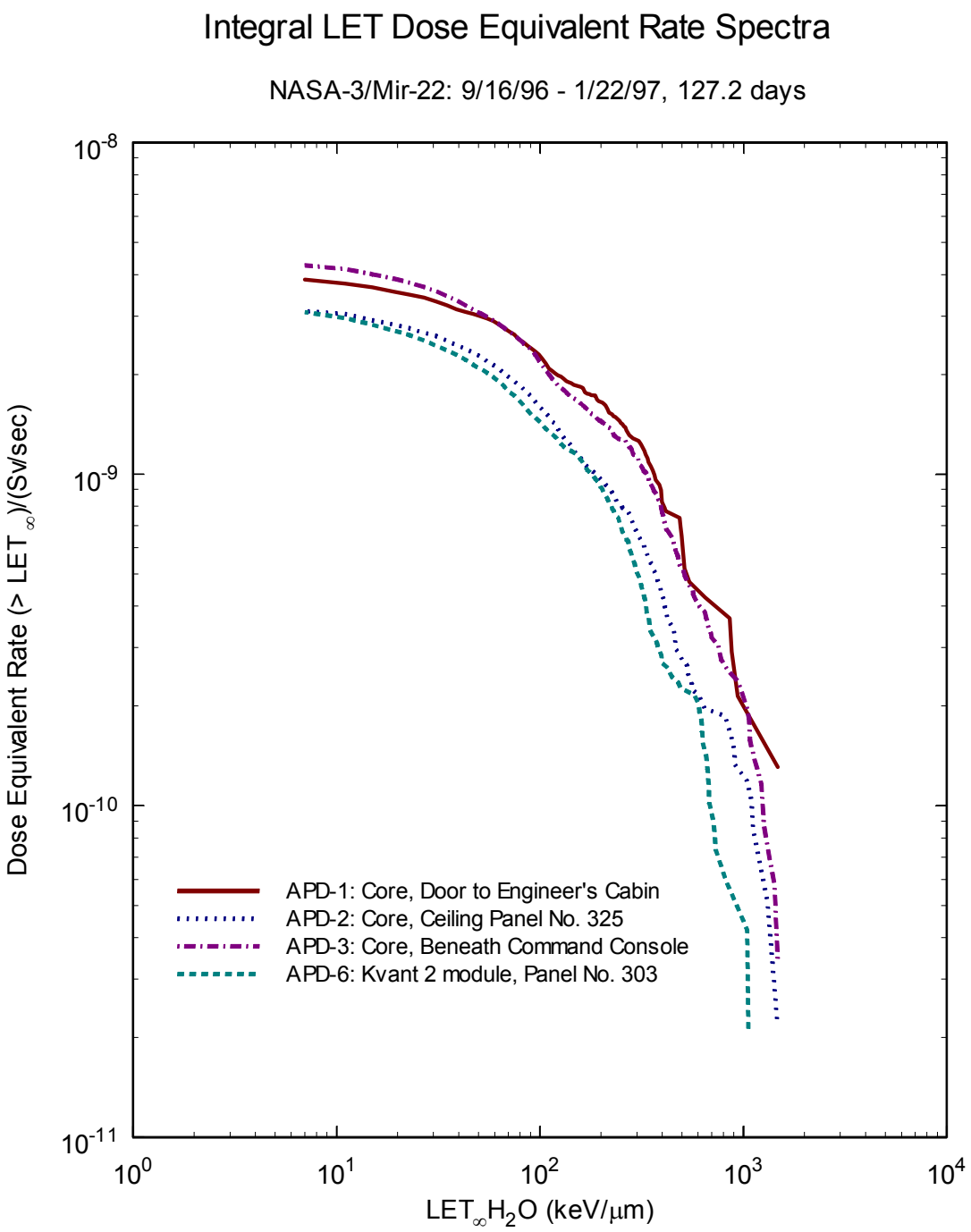

Figure 17. Integral LET dose equivalent rate spectra measured inside the Mir Orbital Station during the NASA-3/Mir-22 mission by the Environmental Radiation Measurements Experiment: 16 September 1996–22 January 1997.

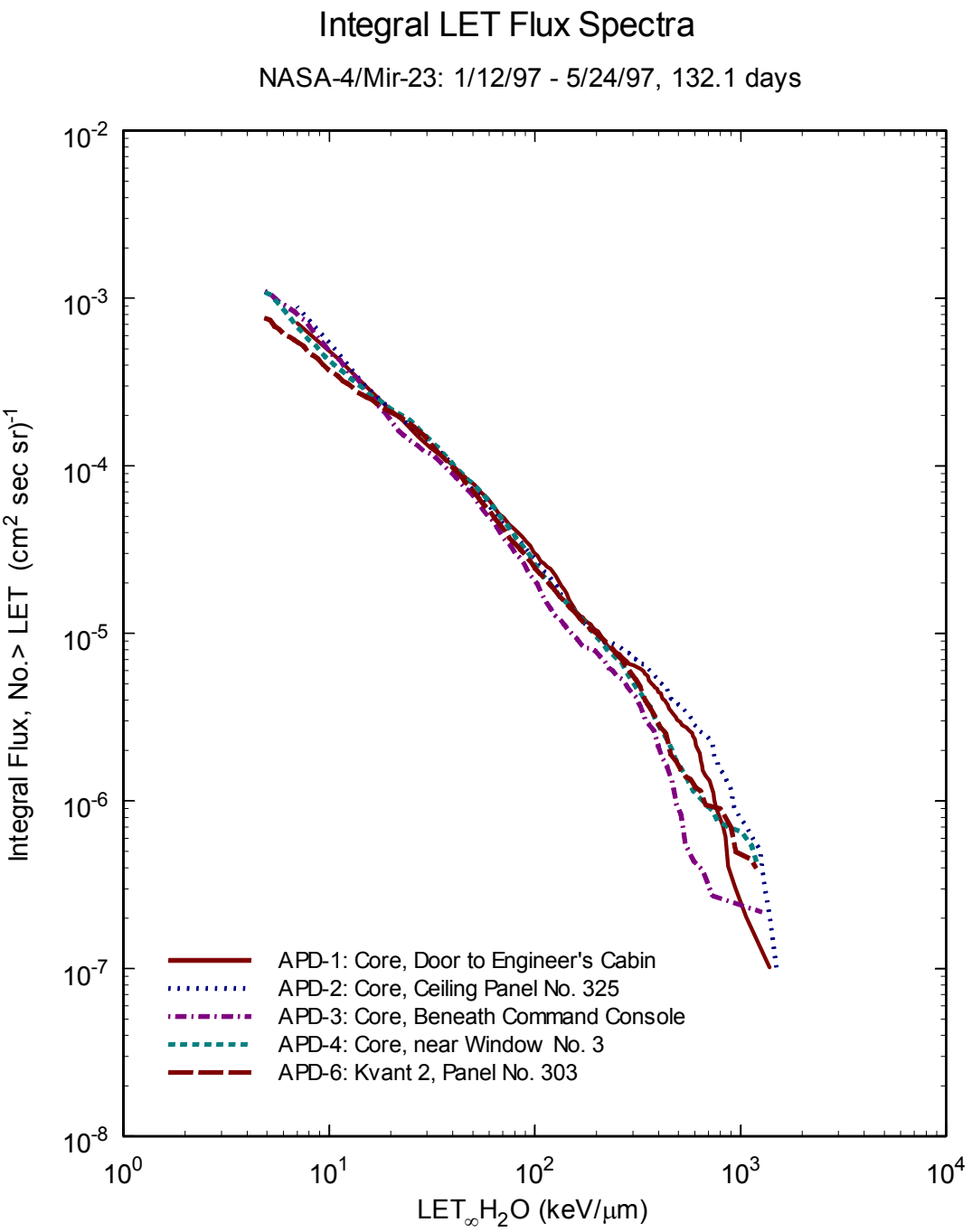

Figure 18. Integral LET flux spectra measured inside the Mir Orbital Station during the NASA-4/Mir-23 mission by the Environmental Radiation Measurements Experiment: 12 January–22 May 1997. APD-6 was exposed for 267.5 days on both the NASA-4/Mir-23 and NASA-5/Mir-24 missions.

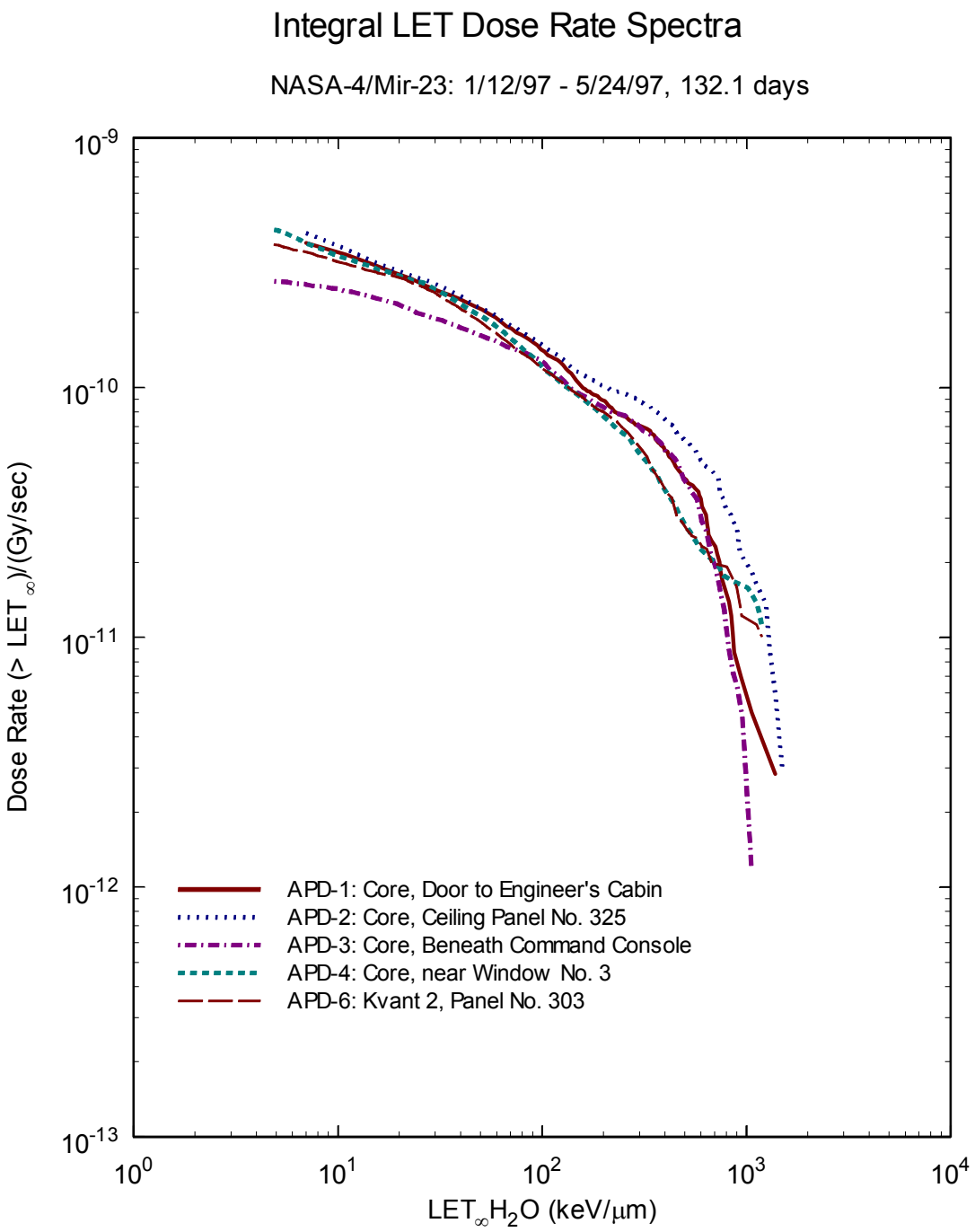

Figure 19. Integral LET dose rate spectra measured inside the Mir Orbital Station during the NASA-4/Mir-23 mission by the Environmental Radiation Measurements Experiment: 12 January–22 May 1997. APD-6 was exposed for 267.5 days on both the NASA-4/Mir-23 and NASA-5/Mir-24 missions.

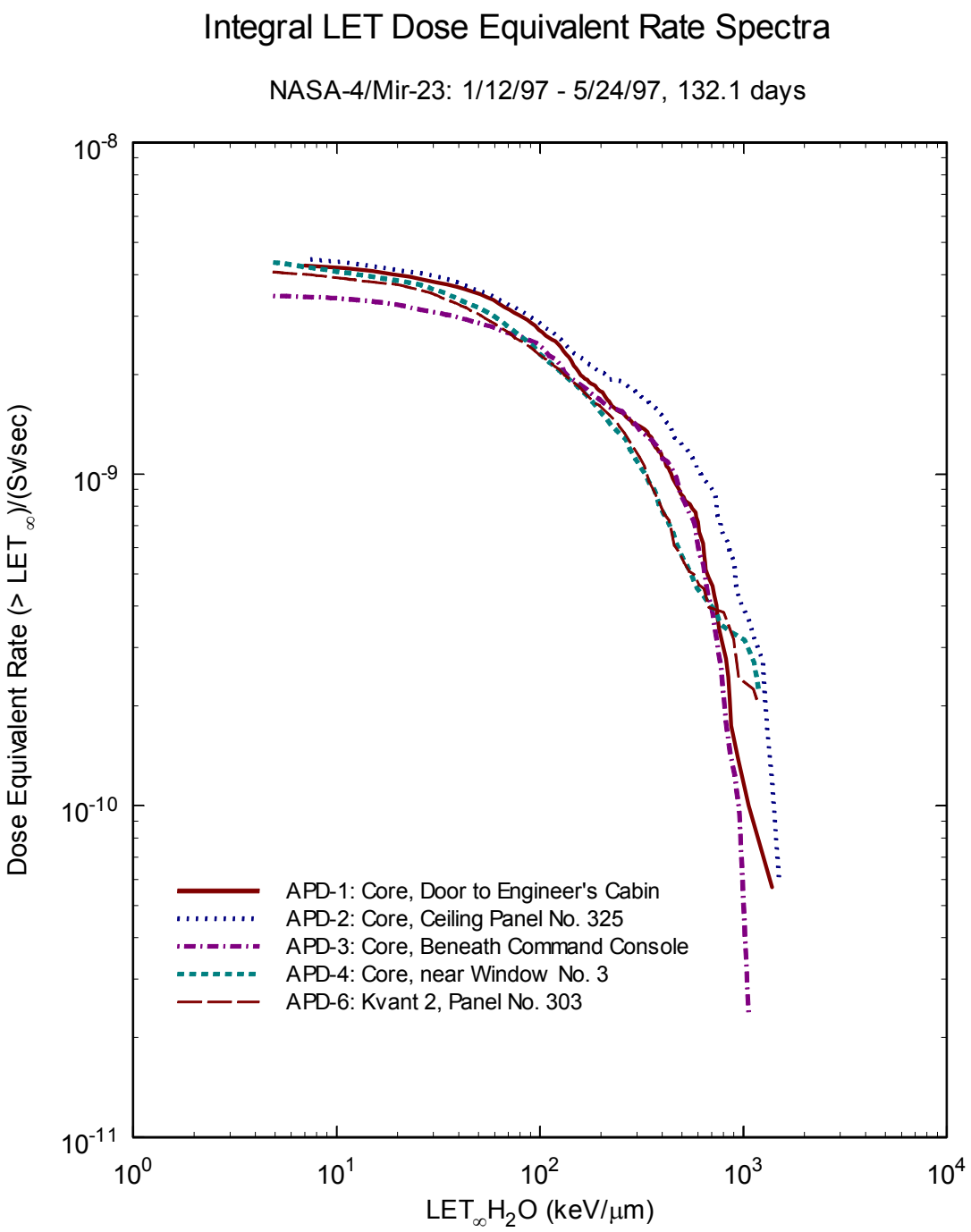

Figure 20. Integral LET dose equivalent rate spectra measured inside the Mir Orbital Station during the NASA-4/Mir-23 mission by the Environmental Radiation Measurements Experiment: 12 January–22 May 1997. APD-6 was exposed for 267.5 days on both the NASA-4/Mir-23 and NASA-5/Mir-24 missions.

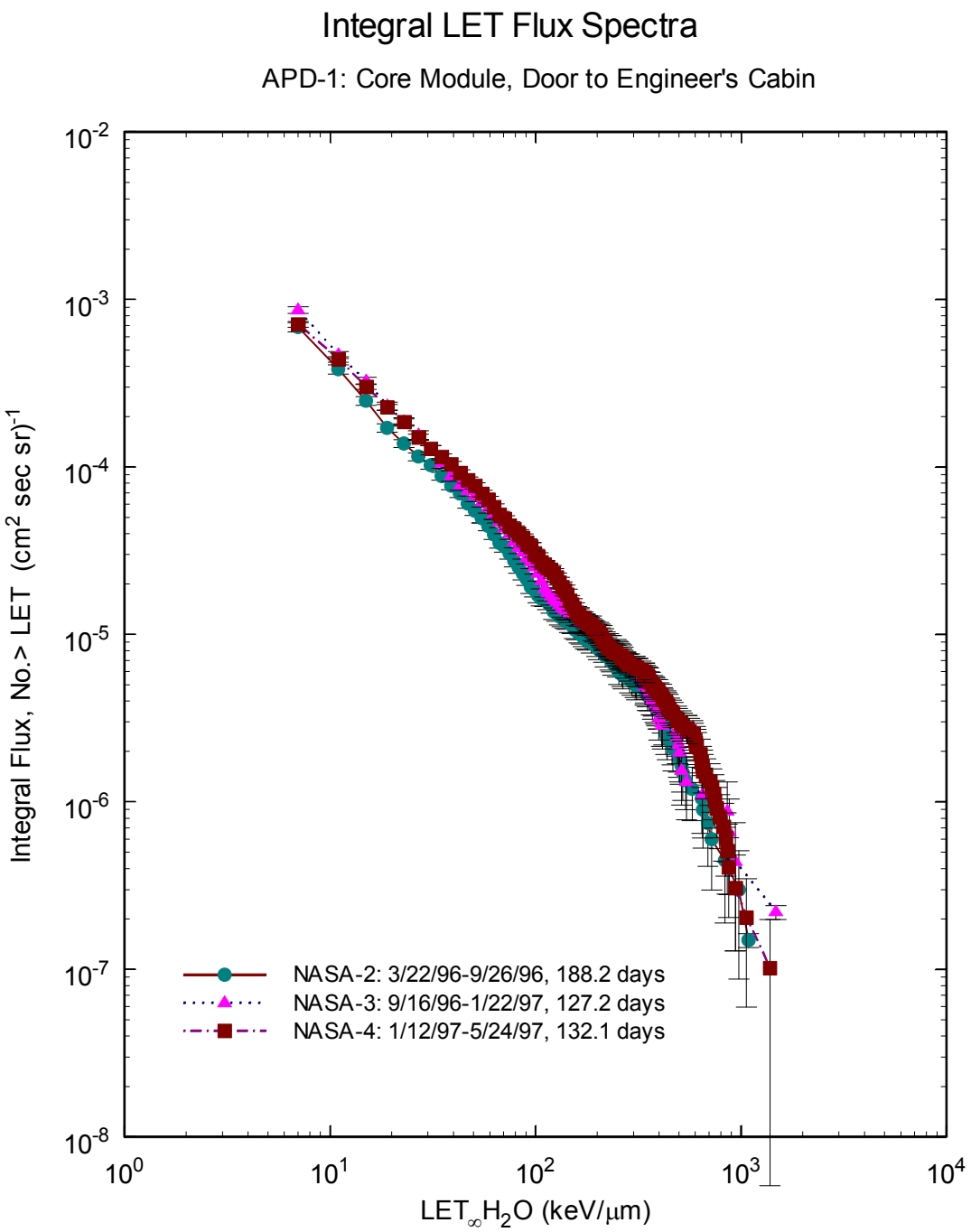

Figure 21. Comparison of Integral LET flux spectra measured at the door to the flight engineer's cabin during the NASA-2/Mir-21, NASA-3/Mir-22, and NASA-4/Mir-23 missions.

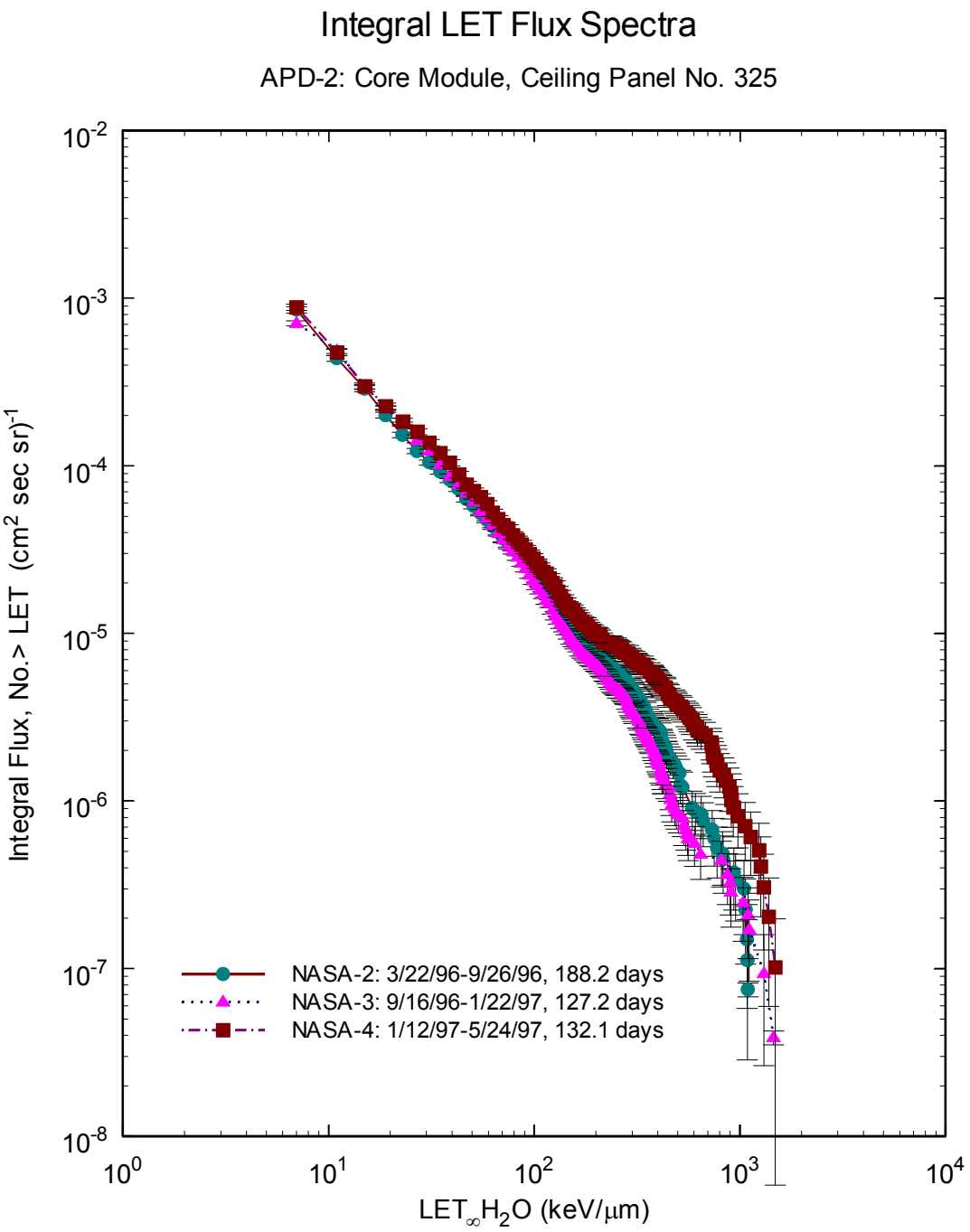

Figure 22. Comparison of Integral LET flux spectra measured near the R-16 Operational Dosimeter on Ceiling Panel No. 325 in the Base Block during the NASA-2/Mir-21, NASA-3/Mir-22, and NASA-4/Mir-23 missions.

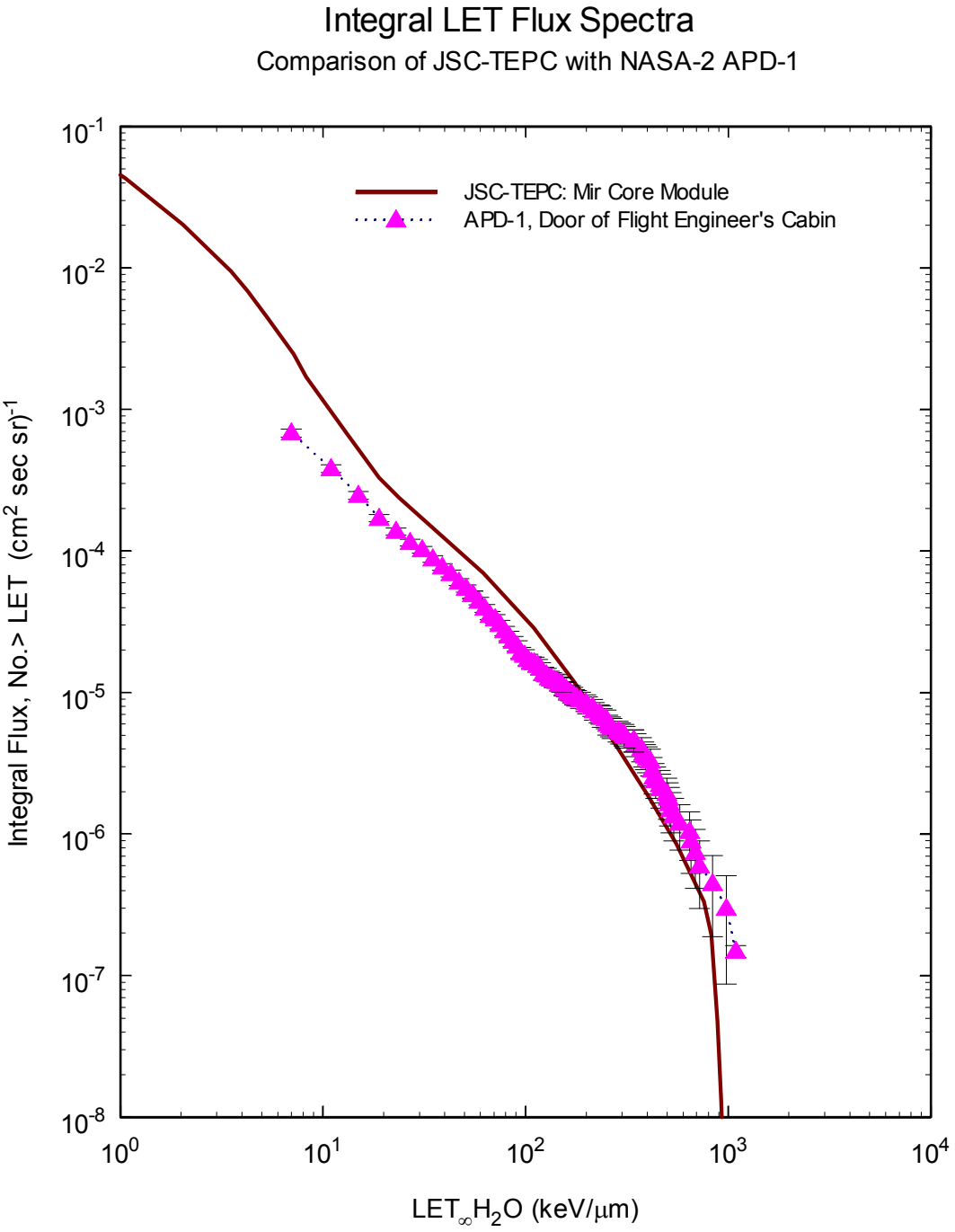

Figure 23. Comparison of Integral LET flux spectra measured inside the Mir Orbital Station during the NASA-2/Mir-21 mission by the USF Environmental Radiation Measurements Experiment and the NASA-JSC Tissue Equivalent Proportional Counter[12].

4.4.3 TOTAL DOSE AND DOSE EQUIVALENT RATES

4.4.3.1 Results from Combined TLD and CR-39 PNTD Measurements

Absorbed doses as measured by TLDs were corrected for high LET efficiency as explained above. Dose and Dose Equivalent for particles of LET ≥5 keV/μm were determined from the integral LET dose rate and dose equivalent rate spectra, respectively, as measured by the CR-39 PNTDs. Mean Quality Factors were determined from the total mean dose rate and dose equivalent rates. Table 10 summarizes the total mean dose rate, mean dose equivalent rate, and the mean quality factor determined from combined TLD and CR-39 PNTD results from the NASA-2/Mir-21 APDs. Also shown in Table 10 are the doses and dose equivalents from particles of LET ≥5 keV/μm and their relative contributions to total dose and dose equivalent rates. Tables 11 and 12 summarize similar results for the NASA-3/Mir-22 and the NASA-4/Mir-23 APDs, respectively. Alternatively, the mean dose rates, dose equivalent rates and mean quality factors measured in each APD by location during the three NASA/Mir missions are tabulated in Table 13.

During the NASA-2/Mir-21 mission, total dose rate varied from 284 μGy/d for APD-6 in the heavily shielded Kvant 2 location to 420 μGy/d for APD-3 in the lightly shielding Base Block location underneath the command console. Dose equivalent rates on this mission ranged from 518 μSv/d to 714 μSv/d, again at the APD-6 and APD-3 locations respectively. The contribution from particles of LET ≥ 5 keV/μm to total dose rate varied from 7.5% for APD-3 to 11.2% for APD-4. It was 11.1% for APD-6. This reflects the larger flux of low LET particles at the low shielding APD-3 location as compared to the larger number of neutron and proton-induced secondaries in the more heavily shielding APD-4 and APD-6 locations. This effect is even more noticeable in looking at the contribution of particles of LET ≥ 5 keV/μm to the total dose equivalent. For APD-3, 45% of the dose equivalent was from particles of LET ≥ 5 keV/μm while for APD-4 it was 52% and for APD-6 it was 50%.

While the higher LET particles make a relatively small contribution to dose, because of their higher LETs, they contribute a substantial fraction of the dose equivalent. The least shielded APD-3 location had the lowest mean quality factor, 1.7, while the mean quality factor for the more heavily shielded APD-4 and APD-6 locations was 1.9 and 1.8 respectively. Because the uncertainty in this estimate is 0.1, the difference in quality factor is probably not significant. However it is interesting to note that the more heavily shielding location produced the higher mean quality factor.

The observation that the least shielded location yielded both the highest mean dose rate and the lowest mean quality factor while the most heavily shielding location produced the smallest mean dose rate and highest quality factor can again be seen in the results from the NASA-3/Mir-22 mission. The mean dose rate at the APD-6 location was again 284 μGy/d, but the mean dose equivalent rate was higher, at 650 μSv/d and the mean quality factor was a correspondingly higher 2.3. This reflects the fact that a larger proportion of the total flux of particles incident on the APD-6 location was in the form of high LET target fragments from proton and neutron secondary reactions and from primary GCR. APD-5, exposed during both the NASA-2/Mir-21 and NASA-3/Mir-22 missions measured highest mean dose rate, 436 μGy/d, and a high mean dose equivalent rate of 715 μSv/d, but had the lowest mean quality factor, 1.6, at the airlock bulkhead of the Kvant 2 module. Like the other lower shielding locations, the airlock bulkhead received a larger flux of low LET particles, principally primary high energy protons in the SAA, than did the more heavily shielding locations.

Change in altitude is probably the single largest factor contributing to the difference in dose rate measured at the same location inside the Mir over an extended period of time. Dose rate increases by roughly a factor of 2 for every 50 km increase in altitude. Since records of the altitude of the Mir Station

as a function of time are, in principal, available, it should be possible to include altitude variation in any attempt to model the dose rate received inside Mir. Figure 24 shows the mean, perigee and apogee altitude of Mir between 7 February 1997 and 1 May 1998. A Progress tanker is used to boost Mir to a mean altitude of ~400 km on a periodic basis. Atmospheric drag then causes the Mir to slowly drop in altitude to a mean altitude of ~380 over the period of a year. Mir altitude data for the whole of the Environmental Radiation Measurements on Mir Station experiment were not available.

During the NASA-4/Mir-23 mission, mean dose and dose equivalent rates were slightly higher than during the previous two missions, with the exception of APD-3. This increase may in part have been to a small increase in altitude of the station. On 15 April 1997 the Mir was boosted from a mean altitude of 385 km to 390 km. While this altitude increase is small, the flux of primary protons in the SAA is highly altitude dependent and even small increases in altitude can lead to noticeable increases in the proton dose. The other cause of the increase in dose rate may be a change in the orientation of the Station. The proton environment in LEO is directionally dependent with the leading edge of the station receiving a higher proton flux than the station's trailing edge.

Information about the orientation of Mir and about the local shielding environment present at a given location are difficult to obtain. Data of Mir's attitude with respect to the Sun is not readily available and it is not know whether records of this parameter have been maintained over the life of the station. The shielding environment inside the station is constantly changing. Over the course of it's history, the Mir has been expanded from the single Base Block to a complex configuration consisting of six separate modules. In addition, much of the scientific research carried out aboard Mir is conducted in the Base Block. This means that much equipment is constantly being moved into and out of the volume near the four Base Block locations in which APDs were located.

As with the two previous missions, the highest dose rate was seen in the least shielded APD-3 location during the NASA-4/Mir-23 mission. Only 6.1% of the dose measured by the APD-3 detector was from particles of LET ≥ 5 keV/μm. Similarly, the dose equivalent at this location was 653 μSv/d as compared to 659 μSv/d in the more heavily shielded APD-4 location. However, particles of LET ≥ 5 keV/μm contributed only 38% of the total dose equivalent in APD-3 as compared to 57% in APD-4. Mean quality factor was 1.7 for APD-3 and 2.1 for APD-4 during NASA-4/Mir-23.

APD-6 Serial No. 0018 remained on board Mir in its heavily shielding location in the Kvant-2 module until the end of the NASA-5/Mir-24 mission in order that it could be compared with the External Dosimeter Array that was deployed during these two missions. Total mean dose rate was 304 μGy/d, mean dose equivalent rate was 624 μSv/d, and mean quality factor was 2.1.

4.4.3.2 Comparison with Results from JSC-TEPC

As mentioned above, during the first part of the NASA-2/Mir-21 mission, the JSC-TEPC was located near the APD-2 location on the ceiling of the Base Block. It was later relocated to the Spektr module. Dose rate and dose equivalent rate measured by the JSC-TEPC are presented in Table 14. The dose rate of 306.6 μGy/d measured by the TEPC while in the Base Block compares favorably to the mean dose rate of 301 μGy/d measured by APD-2 during the NASA-2/Mir-21. However the dose equivalent rate of 770 μSv/d measured by the TEPC is substantially higher than the 555 μSv/d measured by APD-2. Consequently this led to a higher mean quality factor of 2.51 measured by TEPC compared to 1.8 measured by APD-2. Strictly speaking these two sets of measurements are not directly comparable since the TEPC measurements encompass only a subset of the exposure period of the NASA-2/Mir-21 APD-2. Since the TEPC was near the APD-2 location only during the beginning of the NASA-2/Mir-21 mission

and since the altitude of the Mir steadily decreased over the course of the NASA-2/Mir-21 mission, the TEPC measurements represent that time when the Mir was at it highest altitude and, consequently, exposed to its highest flux of trapped protons in the SAA. Dose and dose equivalent rates during the later portion of the NASA-2/Mir-21 mission are expected to have been significantly lower that during the first portion of the mission.

4.4.4 SHIELDING MODEL OF THE MIR BASE BLOCK

A shielding model of the Base Block of the Mir Station was developed by Russian specialists and the shielding probability at nine locations inside the Base Block has been calculated[14]. Three of these nine locations correspond to the placement of APDs 1, 2, and 4. This shielding model is less than ideal in a number of ways. First, it is a model only of the Base Block and does not include shielding effects from the other five modules that make up the final configuration of the Mir Orbital Station. Second, the model is for the Base Block as it was configured at the time of launch in June of 1986. It does not include shielding from the extensive amount of equipment and instrumentation that was later added. Figure 25 shows the three shielding locations inside the Base Block corresponding to APD-1 near the Flight Engineer's Cabin, APD-2 on Ceiling Panel No. 325, and APD-4 in the Adaptor Module near Window No. 14, for which calculations were made. Table 15 lists the spatial coordinates and mean shielding values of these three locations.

Table 10. Measured Dose Rates and Dose Equivalent Rates on the NASA-2/Mir-21 mission (3/22/96-9/26/96, 188.2 days) using TLDs and CR-39 PNTDs, and Contributions to Total Dose Rates and Dose Equivalent Rates from particles, including Target Fragments, of LET ≥ 5 keV/μm.

Detector No.	Location	Dose Rate (μGy/d)	Dose Rate ≥ 5keV/μm (μGy/d)	≥ 5 keV/μm Contribution to Dose	Dose Equivalent Rate (μSv/d)	Dose Equivalent Rate ≥ 5 keV/μm (μSv/d)	≥ 5 keV/μm Contribution to Dose Equivalent	Mean Quality Factor
APD-1	Core, Door to Engineer's Cabin	338 ± 8	26.3 ± 1.2	7.7 %	578 ± 19	261 ± 18	45 %	1.7 ± 0.1
APD-2	Core, Ceiling Panel #325	301 ± 7	29.7 ± 0.8	10.0 %	555 ± 13	278 ± 12	50 %	1.8 ± 0.1
APD-3	Core, beneath Command Console	420 ± 10	31.9 ± 0.8	7.5 %	714 ± 17	319 ± 11	45 %	1.7 ± 0.1
APD-4	Adaptor, near Window #14	339 ± 8	38.0 ± 1.0	11.2 %	646 ± 16	338 ± 13	52 %	1.9 ± 0.1
APD-6	Kvant 2, Ceiling Panel #303	284 ± 7	31.4 ± 0.7	11.1 %	518 ± 11	260 ± 9	50 %	1.8 ± 0.1

Table 11. Measured Dose Rates and Dose Equivalent Rates on the NASA-3/Mir-22 mission (9/16/96—1/22/97, 127.2 days) using TLDs and CR-39 PNTDs, and Contributions to Total Dose Rates and Dose Equivalent Rates from particles, including Target Fragments, of LET ≥ 5 keV/μm.

Detector No.	Location	Dose Rate (μGy/d)	Dose Rate ≥ 5 keV/μm (μGy/d)	≥ 5 keV/μm Contribution to Dose	Dose Equivalent Rate (μSv/d)	Dose Equivalent Rate ≥ 5 keV/μm (μSv/d)	≥ 5 keV/μm Contribution to Dose Equivalent	Mean Quality Factor
APD-1	Core, Door to Engineer's Cabin	325 ± 7	33.2 ± 1.6	10.2 %	626 ± 27	328 ± 26	52 %	1.9 ± 0.1
APD-2	Core, Ceiling Panel #325	286 ± 7	28.0 ± 0.7	9.8 %	526 ± 11	262 ± 9	50 %	1.8 ± 0.1
APD-3	Core, beneath Command Console	396 ± 9	38.9 ± 0.9	9.8 %	724 ± 15	359 ± 12	50 %	1.8 ± 0.1
APD-5*	Kvant 2, airlock bulkhead	436 ± 10	31.5 ± 0.6	7.2 %	715 ± 13	305 ± 14	43 %	1.6 ± 0.1
APD-6	Kvant 2, Ceiling Panel #303	284 ± 7	37.2 ± 0.9	13.1 %	650 ± 16	305 ± 9	47 %	2.3 ± 0.1

*APD-5 was exposed for both the NASA-2 and NASA-3 missions for a total of 305.3 days.

Table 12. Measured Dose Rates and Dose Equivalent Rates on the NASA-4/Mir-23mission (1/12/97—5/24/97, 132.1 days) using TLDs and CR-39 PNTDs, and Contributions to Total Dose Rates and Dose Equivalent Rates from particles, including Target Fragments, of LET ≥ 5 keV/μm.

Detector No.	Location	Dose Rate (μGy/d)	Dose Rate ≥ 5 keV/μm (μGy/d)	≥ 5 keV/μm Contribution to Dose	Dose Equivalent Rate (μSv/d)	Dose Equivalent Rate ≥ 5 keV/μm (μSv/d)	≥ 5 keV/μm Contribution to Dose Equivalent	Mean Quality Factor
APD-1	Core, Door to Engineer's Cabin	341 ± 8	32.7 ± 1.1	9.6 %	678 ± 21	368 ± 18	54 %	2.0 ± 0.1
APD-2	Core, Ceiling Panel #325	307 ± 7	35.9 ± 1.3	11.7 %	656 ± 23	385 ± 21	58 %	2.1 ± 0.1
APD-3	Core, beneath Command Console	375 ± 9	23.0 ± 0.6	6.1 %	653 ± 13	247 ± 16	38 %	1.7 ± 0.1
APD-4	Adaptor, near Window #14	321 ± 7	36.9 ± 1.0	11.4 %	659 ± 21	375 ± 22	57 %	2.1 ± 0.1
APD-6*	Kvant 2, Ceiling Panel #303	304 ± 7	32.3 ± 1.1	10.6 %	624 ± 19	323 ± 19	52 %	2.1 ± 0.1

*APD-6 was exposed for both the NASA-4 and NASA-5 missions for a total of 267.5 days.

Table 13. Mean Dose Rates, Dose Equivalent Rates and Quality Factors measured inside the Mir Orbital Station during the NASA-2/Mir-21, NASA-3/Mir-22, and NASA-4/Mir-23 missions.

APD-1: Mir Base Block, above door to Flight Engineer's cabin. See Figure 7.

Mission	Dates	Duration (days)	Mean Dose Rate (μGy/d)	Mean Dose Equivalent Rate (μSv/d)	Mean Quality Factor
NASA-2/Mir-21	3/22/96-9/26/96	188.2	338 ± 8	578 ± 19	1.7 ± 0.1
NASA-3/Mir-22	9/16/96-1/22/97	127.2	325 ± 7	626 ± 27	1.9 ± 0.1
NASA-4/Mir-23	1/12/97-5/24/97	132.1	341 ± 8	678 ± 21	2.0 ± 0.1

APD-2: Mir Base Block, on Ceiling Panel No. 325 near R-16 Operation Dosimeter and, during the initial part of NASA-2/Mir-21, the JSC-TEPC.

Mission	Dates	Duration (days)	Mean Dose Rate (μGy/d)	Mean Dose Equivalent Rate (μSv/d)	Mean Quality Factor
NASA-2/Mir-21	3/22/96-9/26/96	188.2	301 ± 7	555 ± 13	1.8 ± 0.1
NASA-3/Mir-22	9/16/96-1/22/97	127.2	286 ± 7	526 ± 11	1.8 ± 0.1
NASA-4/Mir-23	1/12/97-5/24/97	132.1	307 ± 7	656 ± 23	2.1 ± 0.1

APD-3: Mir Base Block, beneath Command Console, near Window No. 3. See Figure 8.

Mission	Dates	Duration (days)	Mean Dose Rate (μGy/d)	Mean Dose Equivalent Rate (μSv/d)	Mean Quality Factor
NASA-2/Mir-21	3/22/96-9/26/96	188.2	420 ± 10	714 ± 17	1.7 ± 0.1
NASA-3/Mir-22	9/16/96-1/22/97	127.2	396 ± 9	724 ± 15	1.8 ± 0.1
NASA-4/Mir-23	1/12/97-5/24/97	132.1	375 ± 9	653 ± 13	1.7 ± 0.1

APD-4: Mir Base Block, Docking Adaptor, near Window No. 14. No APD was exposed in the APD-4 location during the NASA-3/Mir-22 mission.

Mission	Dates	Duration (days)	Mean Dose Rate (μGy/d)	Mean Dose Equivalent Rate (μSv/d)	Mean Quality Factor
NASA-2/Mir-21	3/22/96-9/26/96	188.2	339 ± 8	646 ± 16	1.9 ± 0.1
NASA-4/Mir-23	1/12/97-5/24/97	132.1	321 ± 7	659 ± 21	2.1 ± 0.1

Table 13. (cont.)

APD-5: Kvant-2 Module, wall of Airlock Bulkhead. APD Serial No. 0005 was exposed during both the NASA-2/Mir-21 and NASA-3/Mir-22 missions. APD Serial No. 0011 was exposed on both NASA-3/Mir-22 and NASA-4/Mir-23 missions, but was probably moved during changeout of the second for the third batch of APDs.

Mission	Dates	Duration (days)	Mean Dose Rate (μGy/d)	Mean Dose Equivalent Rate (μSv/d)	Mean Quality Factor
NASA-2/Mir-21 NASA-3/Mir-22	3/22/96-1/22/97	305.3	436 ± 10	715 ± 13	1.6 ± 0.1

APD-6: Kvant-2 Module, on Ceiling Panel No. 303. APD Serial No. 0018 remained on Mir during both the NASA-4/Mir-23 and NASA-5/Mir-24 missions to serve as an internal control for the External Dosimeter Array exposure.

Mission	Dates	Duration (days)	Mean Dose Rate (μGy/d)	Mean Dose Equivalent Rate (μSv/d)	Mean Quality Factor
NASA-2/Mir-21	3/22/96-9/26/96	188.2	284 ± 7	518 ± 11	1.8 ± 0.1
NASA-3/Mir-22	9/16/96-1/22/97	127.2	284 ± 7	650 ± 16	2.3 ± 0.1
NASA-4/Mir-23 NASA-5/Mir-24	1/12/97-8/22/97	267.5	304 ± 7	624 ± 19	2.1 ± 0.1

Table 14. Dose and Dose Equivalent Rates measured by the JSC-TEPC during the NASA-2/Mir-21 mission[12].

Measurement	Dose Rate (μGy/d)	Dose Equivalent Rate (μSv/d)	Mean Quality Factor <Q>
JSC TEPC, Core Module	306.6	770	2.51
JSC TEPC, Spektr Module	369.2	874.2	2.37

Table 15. Coordinates of Locations inside the Mir Core Module for which Shielding Distributions were Calculated. Origin (0,0,0) is located at the front of the adapter module, and the centerline of the station[14].

Location No.	Description	*x* (cm)	*y* (cm)	*z* (cm)	mean shielding (g/cm^2)
1	Engineer's cabin, outer wall	945	40	–190	22
2	Panel No. 325, near R-16 Dosimeter	796	204	0	44
4	Adapter Module, near Window No. 14	80	0	72	38

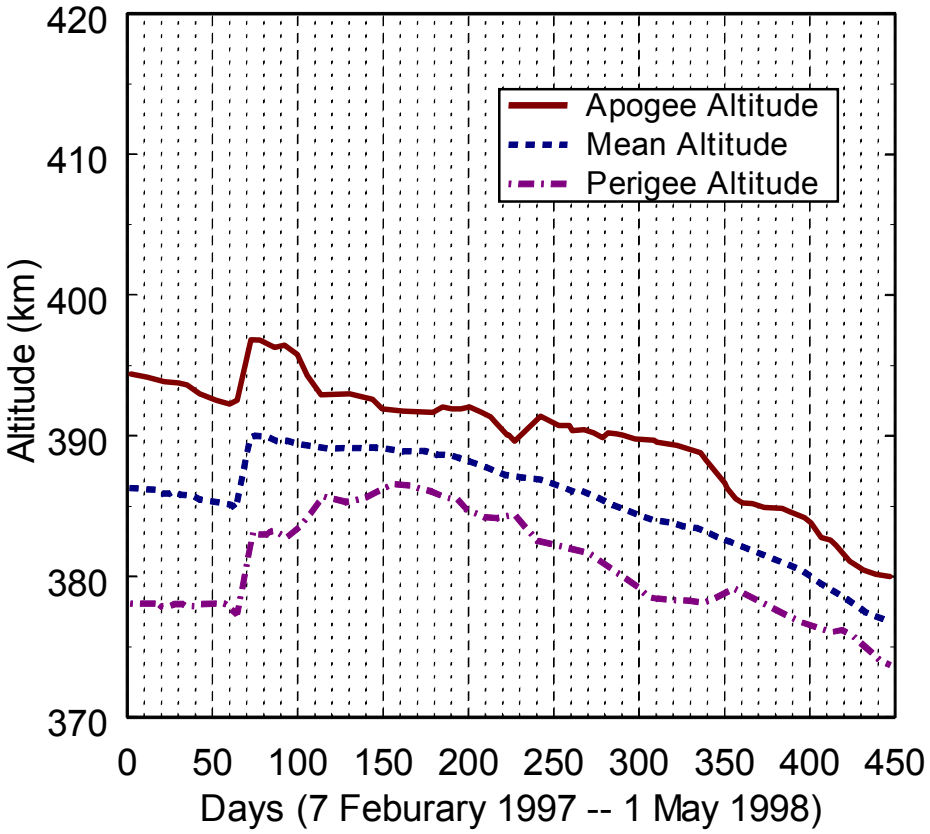

Figure 24. Altitude of the Mir Orbital Station during the NASA-4/Mir-23, NASA-5/Mir-24, and NASA-6/Mir-25 missions. On 4/15/97 Mir was boosted from a mean altitude of 385 km to 390 km[15].

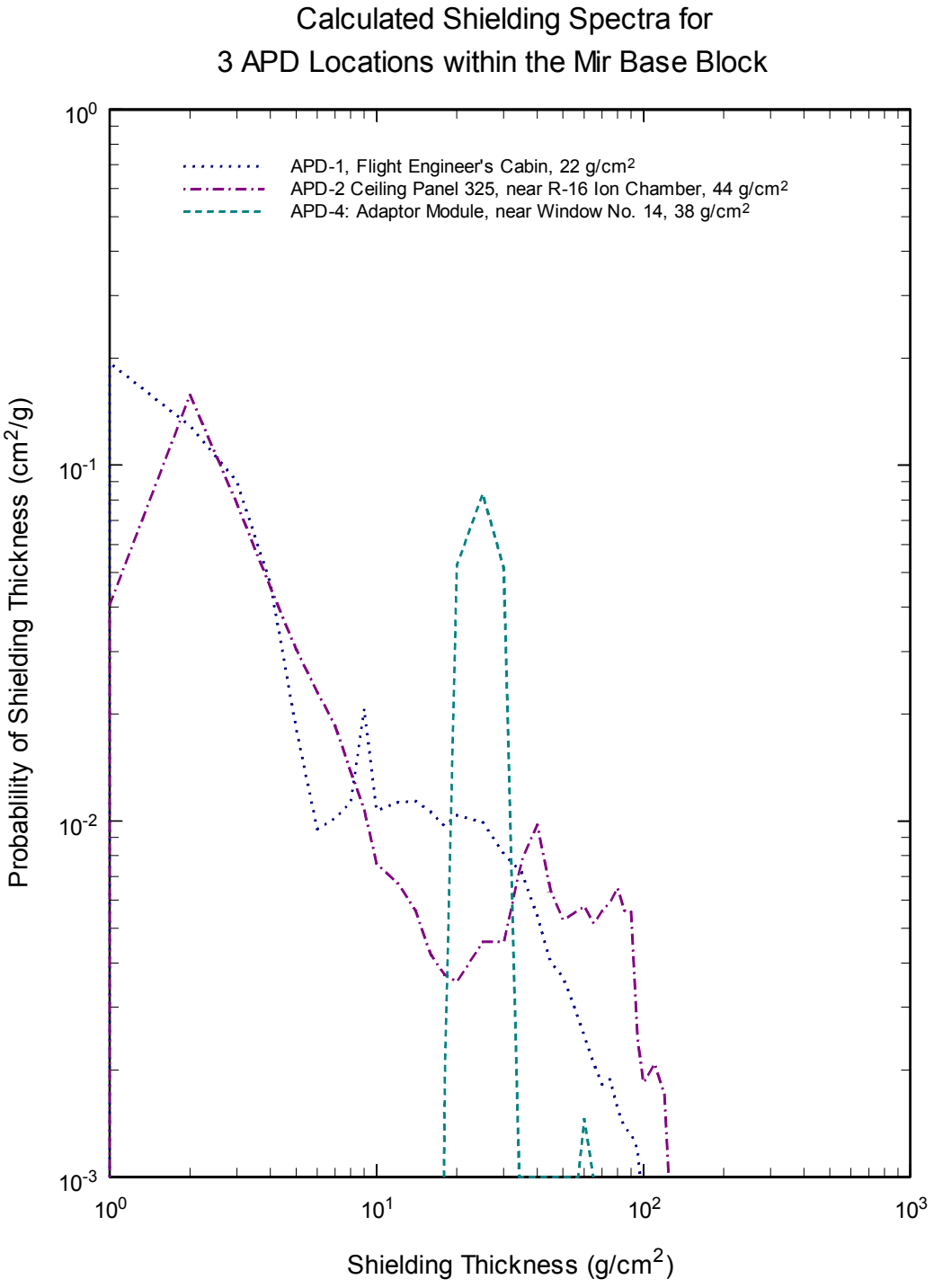

Figure 25. Calculated shielding probabilities for three APD locations inside the Mir Base Block[adapted from 14].

5. FBI-4: EXTERNAL EXPERIMENT

The purpose of the external experiment was to measure absorbed dose as a function of shielding and LET Spectra on the outer surface of the Mir Station during Solar Minimum. To achieve this objective an External Dosimeter Array (EDA) was designed and fabricated with the aid of NASA Ames Research Center, NASA Johnson Space Center, the Institute of Biomedical Problems, Moscow, and RSC Energia. The measurements made with the EDA compliment a similar set of measurements made at the same location on the outside of the Mir Orbital Station in 1991 during Solar Maximum.

5.1 Design of the External Dosimeter Array

The External Dosimeter Array (EDA) consisted of two sets of passive radiation detectors, one provided by the University of San Francisco (USF) and the other by the Institute of Biomedical Problems (IMBP), Moscow. The USF detector set contained two sets of thin TLD stacks to measure dose as a function of shielding depth under low shielding and two sets of CR-39 Plastic Nuclear Track Detectors (PNTDs) to measure the LET spectra ≥5 keV/μm external to the Mir station. The IMBP detector package consisted of six stacks of TLDs to measured dose as a function of shielding depth and one stack of PNTDs. The EDA is pictured in Figure 26. The EDA assembly measures 34 cm × 16 cm × 12 cm and has a mass of 1.78 kg. The EDA interfaces with the stationary STD platform currently mounted on the exterior of the Kvant 2 module. The STD platform was developed by the Russians and previously deployed. Similar radiation experiments have been carried out by the Russian specialists using the STD platform in June 1991.

The USF dosimeters consisted of two aluminum canisters (5 cm diameter, 0.95 cm thick) containing CR-39 PNTDs and a TLD block (6.0 cm × 3.5 cm × 2.0 cm). The CR-39 canisters had a 2 cm diameter Kapton thin-shielding windows on top. The TLD block contained two stacks of TLDs mounted inside 1 cm diameter holders and covered by thin-shielding Kapton windows. The PNTD capsules and TLD block were mounted on a hollow Aluminum plate (12.0 cm × 10.0 cm × 3.0 cm) which in turn was mounted on the front of the EDA base. A 12.0 cm × 10.0 cm × 4.0 cm protective cover was placed on top of the Aluminum plate and covered the PNTD canisters and TLD block while the EDA was stowed on the interior of Mir Station prior to and following external exposure. The protective cover was held in place by means of mechanical clips. Figure 27 shows the assembled EDA platform prior to launch.

The TLD stacks consisted of approximately 20 thin (0.0036") and 12 thick (0.035") TLD-700 (^{7}LiF) chips mounted in a cylindrical Lexan holder. Each TLD chip measured 0.125" on a side. The Lexan holder was covered by a thin layer of aluminized Kapton that provided protection with a minimum of shielding. Two TLD stacks were mounted in an Al block that was, in turned, mounted on the EDA platform (pictured in Figure 27).

The CR-39 PNTDs took the form of 3.33 cm diameter disks. Approximately 16 layers of 600 μm thick CR-39 were separated by layers of 8 μm thick polycarbonate foil. The stacks were placed in Al capsules having two layers of Aluminized Kapton film on the top for protection. Because CR-39 must be in the presence of oxygen to function properly, the capsules were sealed using rubber o-rings. The sealed capsules were then attached to the EDA platform.

The Russian dosimeter package, supplied by the IMBP, consisted of two aluminum containers assembled as one unit. The smaller container (7.2 cm × 2.0 cm × 2.3 cm) contained six stacks of TLDs. The larger container (10.0 cm × 6.5 cm × 4.2 cm) contained PNTDs together with holders containing TLDs. The tops of each container are covered by thin Kapton windows.

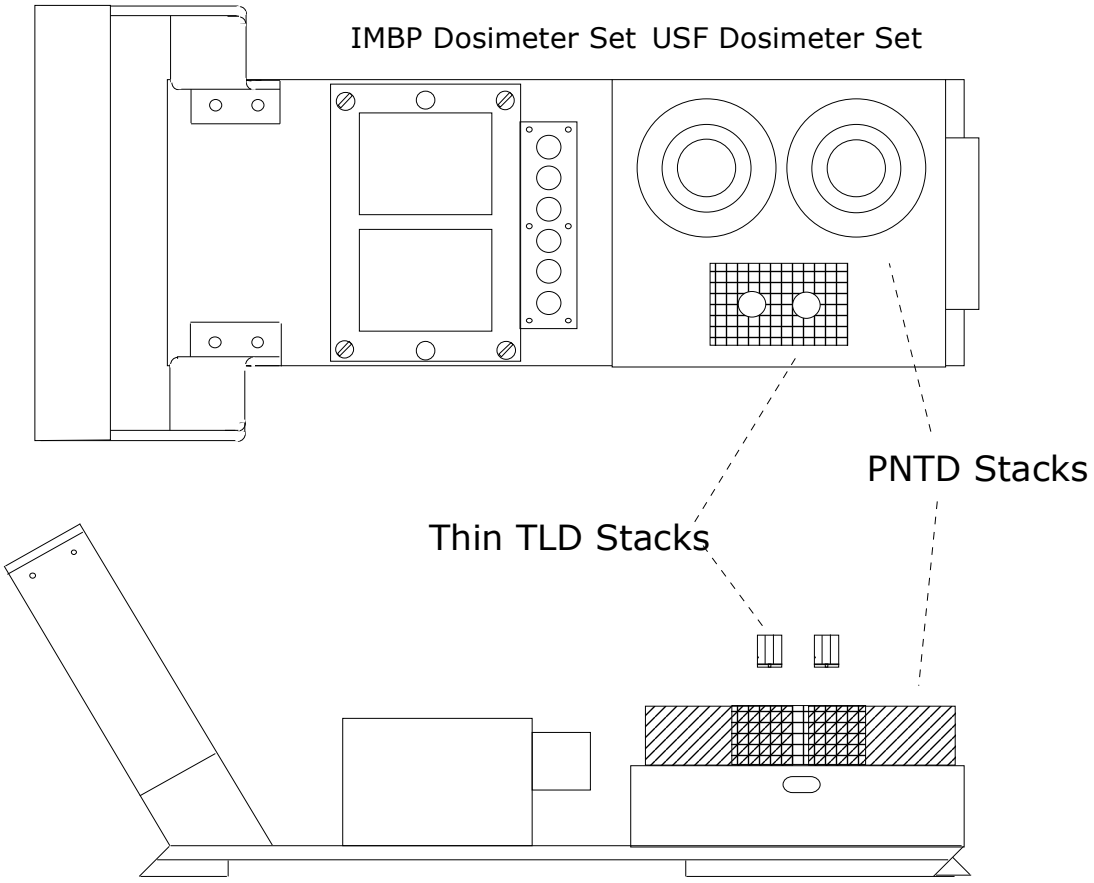

Figure 26. Diagram of the External Dosimeter Array showing the location of the two USF TLD stacks to measure dose as a function of shielding depth and the two CR-39 PNTD stacks to measure LET spectra.

The EDA was exposed externally while attached to the STD platform on top of two gyrodynes on the Kvant 2 module. Figure 28 shows the location of the two gyrodynes. The STD platform is part of the cover of these two gyrodynes. The EDA possesses a spring-loaded lock at the bottom of the front end which fitted in the STD platform. During EVA the EDA was grasped and maneuvered by the astronauts and cosmonauts via the white Aluminum handle shown in Figure 27.

5.2 Deployment, Exposure and Retrieval of the EDA

The EDA was delivered to Mir during the STS-81 Shuttle mission. On 29 April 1997, the EDA was deployed by U.S. Astronaut Jerry Linenger during his EVA. It was retrieved during the EVA of Mike Foale on 5 September 1997. The EDA was returned to Earth by STS-86 on 5 October 1997 at the conclusion of the NASA-5 mission.

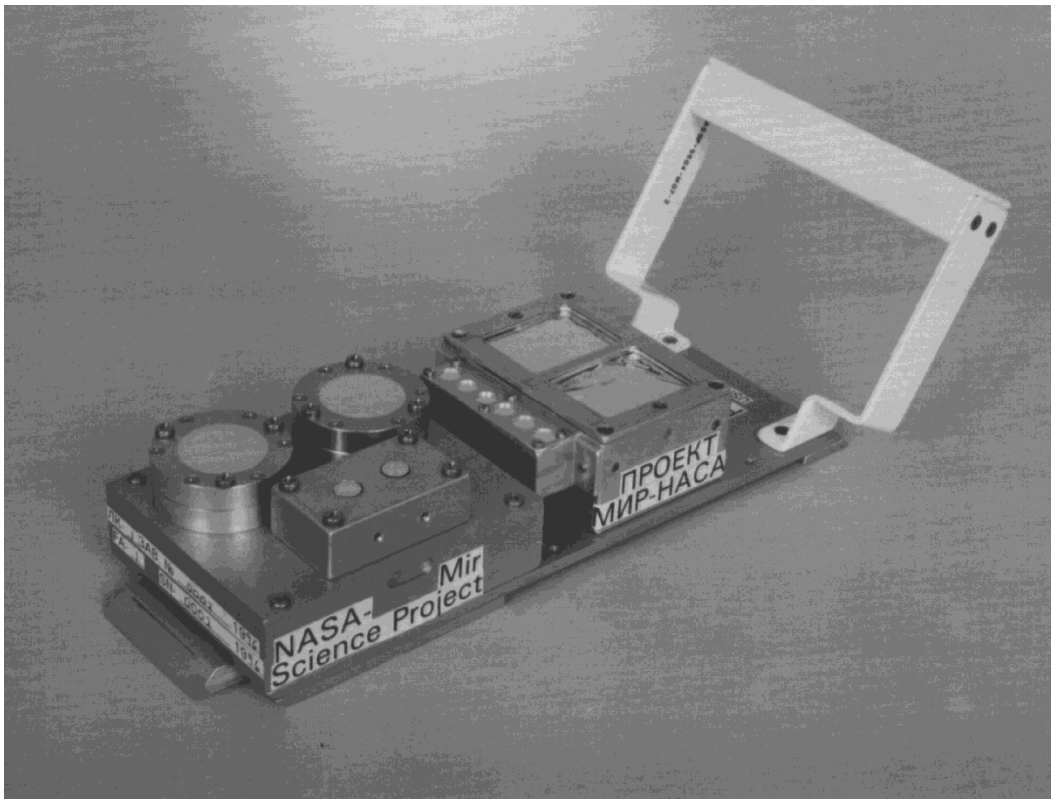

Figure 27. The assembled EDA prior to launch on STS-81. The USF PNTDs are contained in the larger diameter capsules at front, while the TLD stacks are inside the Al block at front. The detector package of IMBP is at the back, near the handle.

Prior to external deployment and following retrieval of the EDA from the STD platform, it was stored in the heavily shielded Ceiling Panel No. 303 location inside the Kvant 2 module. This location in the interior of the Kvant 2 module roughly corresponds to the external location of the STD platform near the airlock of the Kvant 2 as illustrated in Figure 28. Ceiling Panel No. 303 was also the location of APD-6, which served as an internal control during the external exposure of the EDA. The total external exposure of the EDA lasted 130.1 days while its total time aboard Mir lasted 267.2 days (NASA-4/Mir-23 and NASA-5/Mir-24 missions).

5.3 Analysis of the EDA Detectors

5.3.1 READOUT OF TLDS

Following the return of the EDA to the Earth, the TLD stacks were removed from the EDA and read out. Each TLD was individually read out using a Harshaw 4000 TLD reader. A ground control stack of TLDs, identical to that exposed on the EDA was read out at the same time. Following readout, each TLD from both the flight and ground control stacks was individually calibrated using a NIST certified ^{137}Cs γ-ray source and the TLDs were read out again. Dose values were corrected for the background dose accumulated in the ground control stack. Dose was determined as a function of the order of the TLD chips in the stack. The order of the TLD was then converted to depth in LiF, the TLD material, in units of g/cm^2.

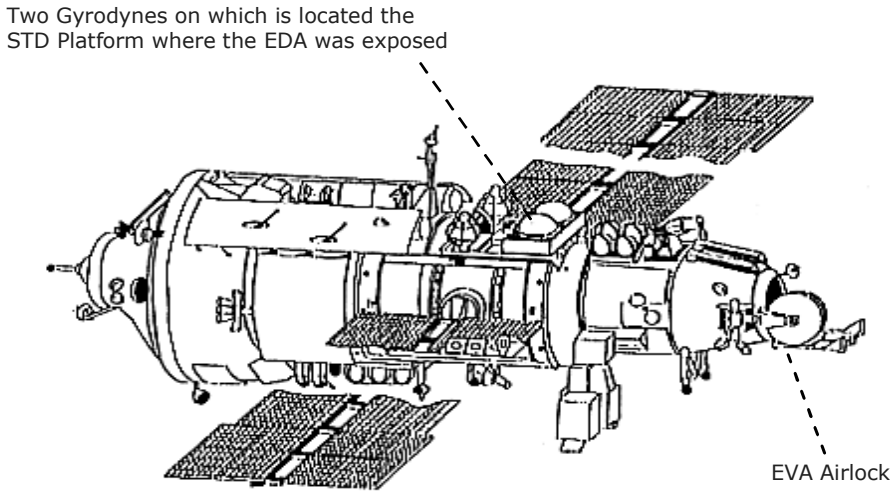

Figure 28. Location of the EDA experiment on the Kvant 2 modules. The STD platform in which the EDA was exposed is part of the cover of the two gyrodynes.

5.3.2 PROCESSING, READOUT AND ANALYSIS OF CR-39 PNTDS

Following receipt of the exposed EDA, the two Aluminum capsules containing the CR-39 stacks were removed from the EDA tray and opened. While they were being opened, observation was made to see if the capsules were under a different pressure than the ambient environment, in order to determine if the oxygen environment had remained during exposure or had diffused out into vacuum. Unfortunately, it was not possible to determine whether the seal had remained effective or not. The uppermost Kapton layer of one of the two capsules appeared to have started loosening. However since the CR-39 layers were protected by two, individually sealed, Kapton layers this didn't necessarily mean the CR-39 was subjected to vacuum.

Processing of the CR-39 layers was carried out in 6.25 *N* NaOH at 50°C. Because the uppermost layer of CR-39 was under extremely low shielding, the fluence of particles was expected to be extremely high, and it was possible that the least shielded layer of CR-39 was saturated with tracks. In order to maintain small track size, thereby minimizing the amount of track overlap, chemical processing of the uppermost layer was carried out for only 24 hours. The remaining layers were processed for a period of 36 hours.

5.4 Results from the EDA Detectors

5.4.1 DOSE AS A FUNCTION OF SHIELDING DEPTH

Dose rate measured in the thin TLD stacks as a function of shielding depth is shown in Figure 29. The two lower curves in Figure 29 are the results of the FBI-4 measurements. Dose rate can be seen to decrease from ~100 cGy/d at 0.01 g/cm^2 to ~0.1 cGy/d at 1 g/cm^2. On the exterior surface of Mir, much of the flux of charged particles takes the form of low energy electrons and protons. Within the first g/cm^2 of shielding, this low energy flux is attenuated by nearly three orders of magnitude. Deeper than 1 g/cm^2 dose rate tends to level off. This is partly due to the fact that shielding from the above direction (the TLDs stacked above) is now similar to the shielding from other directions (mostly the sides).

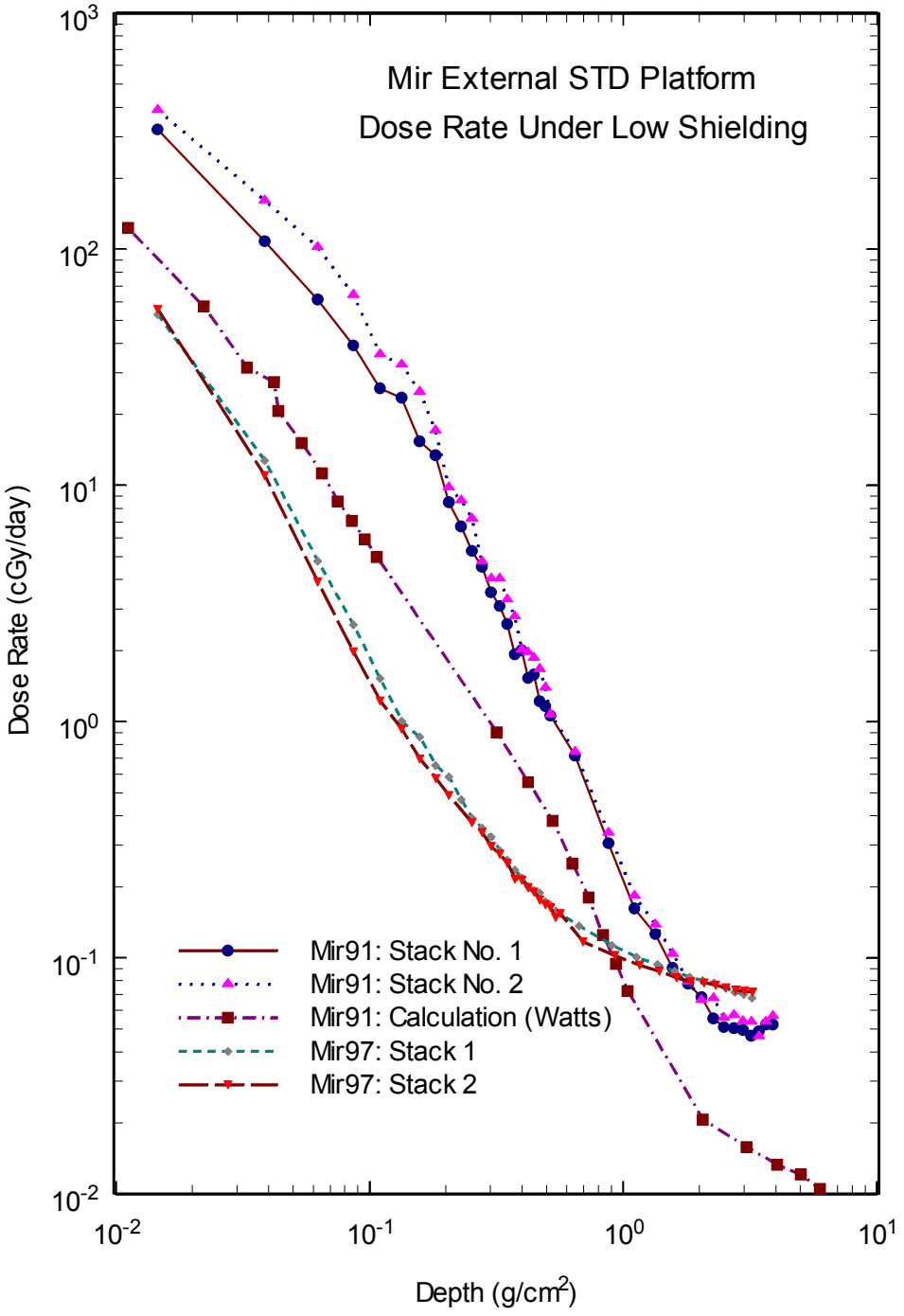

Figure 29. Dose as a function of shielding depth measured on the external surface of Mir during the NASA-4/Mir-23 and NASA-5/Mir-24 missions. Also shown are measurements made at the same location in 1991 and a model calculation for the 1991 measurement[10].

Also shown in Figure 29 are the results from an earlier measurement of dose as a function of depth carried out on the outside of the Mir station in June, 1991[10]. The first measurement was made at a time roughly corresponding to Solar Maximum. This set of exposures lasted approximately 27 days. The second set of measurements was carried out beginning on 29 April 1997 and ending on 5 September 1997, a period roughly corresponding to Solar Minimum. Total duration of the second set of exposure is was 130 days. The 1991 measure are approximately one order of magnitude greater than the NASA-4/5 measurements over the range of shielding thickness measured. The difference in the two sets of measurements is partially explained by the different solar cycle conditions.

A model calculation of the 1991 measurement made using the AP8MAX trapped proton code is shown by the square symbols. The model calculation also lies below the 1991 curves. the 1991 measurements followed on the heels of several large solar particle events (SPE) which created new trapped particle belts. These belts were first identified by the SAMPEX satellite and contributions from these belts led to the 1991 measurements being greater than the model calculations. While the two sets of measurements (1991 and NASA-4/5) were made at solar maximum and solar minimum respectively, they cannot be considered upper and lower limits of the dose rate vs. shielding as a function of solar cycle due to the elevated levels in the trapped particles exposures due to SPE in the 1991 measurements.

Figure 30. Early photograph of Mir and Kvant 2 taken prior to June 1991, when the external exposure was made on the Kvant 2 STD platform. The shielding environment immediately surrounding the STD platform is significantly different to what it was in 1997, since the Spektr and Priroda modules had yet to be added. The STD platform is partly shielded by the solar panel attached to the Base Block.

While the EDA tray was of the same design during both experiments, the composition and arrangement of passive detectors and their holders differed between the two exposures. The original EDA used during the June 1991 experiment was never returned to Earth, and no drawings or photographs of the original experiment could be located. Thus there are probably differences in shielding between the two exposures. Differences in the two exposures also arise from the fact that the Mir only possessed the Base Block, Kvant 1, Kvant 2 and Kristal modules during the 1991 exposure. Figure 30 is an early photograph of the

Mir Orbital Station with Kvant 2 module. The STD platform is partly shielded by a solar panel attached to the Base Block and running parallel to the length of the Kvant 2 module. By 1997, the Spektr and Priroda modules had been added and the arrangement of the older modules was modified to accommodate the newer ones. In addition, it is possible that the station orientation was different for the two exposure times. These measurements were as nearly as possible carried out under identical conditions except for solar epoch. Duration of the exposures, time spent inside Mir both before and after exposure, etc. were beyond the control of the principal investigator.

5.4.2 RESULTS FROM CR-39 PNTDS

Like the Dose/Depth profiles made with the TLD stacks, the CR-39 PNTDs showed a rapid decrease in signal as a function of depth in the stack. The uppermost layer of CR-39 was saturated with many stopping proton tracks and was not able to be measured. Figure 31 shows photomicrographs of four CR-39 layers from the EDA CR-39 stack. All photomicrographs were taken at a magnification of 600×.

The photo in the upper left of Figure 31 is from the uppermost detector. The granulated appearance of the surface surrounding the pointed track is caused by the many overlapping tracks of stopping particles, mostly protons. Because the tracks are overlapping, it wasn't possible to measure the LET spectrum since the track diameters couldn't be discerned. Even the very short etching duration of 24 hours was not short enough to prevent the tracks from merging. Had the etching been any shorter, it wouldn't have been possible to see the tracks due to their small size.

The photomicrograph in the upper right corner of Figure 31 is of the second layer of CR-39. While there is still a high density of shallow tracks from stopping particles, the tracks no longer overlap and it is possible to make out their perimeters and, thus, accurately measure them. The two bottom photomicrographs in Figure 31 are from the fourth and eighth layers, respectively. Here the track density was quite low and no longer appeared to be changing as a function of depth. The tracks visible in the photomicrographs are from primary charged particles and from stopping secondary particles.

The track density in the more heavily shielded layers of the external CR-39 stacks was lower than expected, especially when compared to that measured on the inside of Mir in APD-6. One possibility its that the oxygen in the CR-39 capsule diffused out during exposure. If oxygen is not present when a charged particle forms a latent damage trail in CR-39, chemical recombination along the latent damage trail causes it to quickly fade. It is possible that many of the tracks in the EDA CR-39 detectors faded while the EDA was still on the outer surface of the Mir. CR-39 layers from the other capsule will be examined in order to see if it also possesses the same low track density.

The integral LET spectrum was measured on the second CR-39 layer and is shown in Figure 32. Also shown in the plot is the integral LET flux spectra measured by the APD-6 which was exposed at a location inside the Kvant 2 module corresponding the location of the EDA outside Mir and which served as an internal control during the external exposure. Both spectra contain only the high-LET component measured in the CR-39 PNTDs that were processed for 36 hours. While the spectrum measured in the externally exposed detector lie above that measured on the inside of Mir, the difference in the two curves is not as great as was expected. This might be partly due to the fading caused by oxygen diffusion out of the CR-39 capsule during the external exposure. Another possibility is that, at higher LETs, the attenuation of the GCR flux by the shielding of the spacecraft is offset by the production of short-range high-LET target fragments produced in interactions between high-energy trapped protons and the nuclei of the stopping medium. At lower LET (<30 keV/μm) the externally exposed detector does lie well above the

internally exposed detector, illustrating the effect of attenuation of the low LET particle flux by the spacecraft shielding.

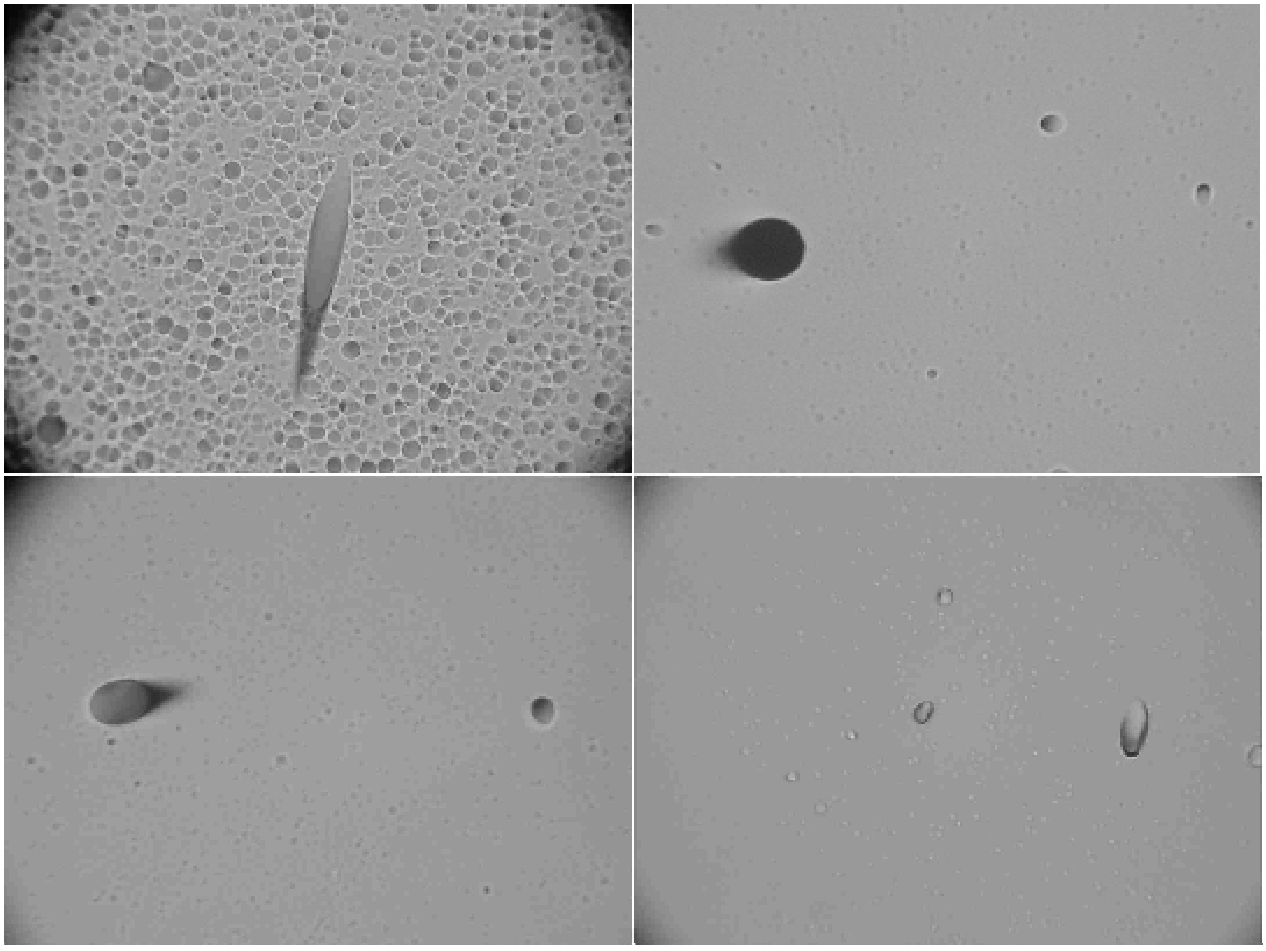

Figure 31. Photomicrographs of CR-39 track detectors exposed on the EDA during the NASA-4/Mir-23 and NASA-5/Mir-24 missions. Clockwise starting in the upper left is the first, second, fourth and eighth layers. The first, top most layer was processed for 24 hours while the other three layers were processed for 36 hours. All photomicrographs were taken at a magnification of 600×.

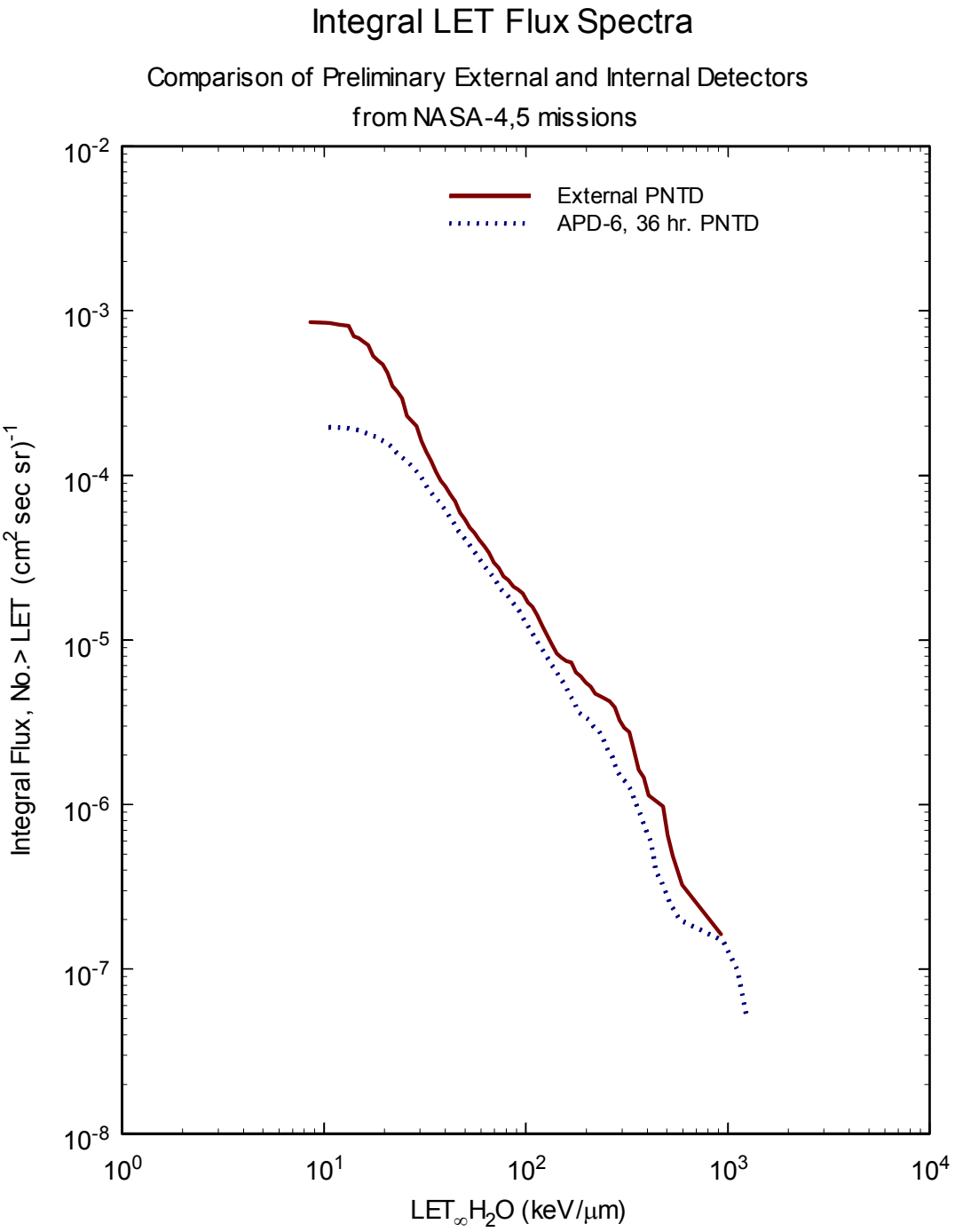

Figure 32. LET Flux Spectra measured on the External Surface of the Kvant 2 module during the NASA-4/5 mission. Also shown is the 36 hr. (high LET) spectrum measured in APD-6 during the same time period.

6. DISCUSSION AND CONCLUSIONS

6.1 FBI-3 Internal Experiment

The FBI-3 internal portion of the Environmental Radiation Measurements on Mir Station experiment was an unqualified success, achieving the vast majority of its objectives. It was fully successful in meeting its primary objective of measuring the total dose and dose equivalent rates at six locations on the interior of the Mir Orbital Station during the NASA-2/Mir-21, NASA-3/Mir-22 and NASA-4/Mir-23 missions. The only anomalies regarding this experiment occurred when a small number of the APDs were mistakenly returned to ground prior to exposure while several other APDs were exposed for more than one mission. All the TLDs and CR-39 PNTD layers functioned properly during the experiment and good quality data was obtained from all detectors. All TLDs yielded doses in the appropriate ranges, consistent with expectations, and LET spectra was measured on all processed CR-39 layers.

Total absorbed dose rate on the NASA-2/Mir-21 mission varied from a low of 284 μGy/d measured by APD-6 in a heavily shielded Kvant-2 location to a high of 420 μGy/d in APD-3 located near the outer wall of the Base Block. Dose equivalent rate similarly ranged from 518 μSv/d for APD-6 to 714 μSv/d for APD-3. Mean quality factor in all five NASA-2/Mir-21 APDs was roughly the same, ranging from 1.7 to 1.9 with an experimental uncertainty of 0.1.

Differences in dose rate, dose equivalent rate and mean quality factor were somewhat larger amongst the measurements made during the NASA-3/Mir-22 mission. As in the previous mission, the lowest dose rate, 284 μGy/d, was measure in the Kvant-2 APD-6. However, the lowest dose equivalent rate was measured in the Base Block: 526 μSv/d in APD-2. The highest dose and dose equivalent rates were once again measured in APD-3: 396 μGy/d and 724 μSv/d, respectively. While APD-6 had the lowest dose rate, it also possessed the highest mean quality factor: 2.3 ± 0.1. This was the highest mean quality factor measured during the whole of the FBI-3 experiment and is comparable to the mean quality factors of between 2.3 and 2.5 measured by the JSC-TEPC while aboard Mir.

The highest dose rate and lowest mean quality factor were measured in APD-5, which was mistakenly exposed during both the NASA-2/Mir-21 and NASA-3/Mir-22 missions. APD-5 was located on the wall of the airlock bulkhead in the Kvant-2 module, a location with a relatively small amount of shielding. APD-5 measured a dose rate of 436 μGy/d, a dose equivalent rate of 715 μSv/d, and a mean quality factor of 1.3.

Mean quality factor during the NASA-4/Mir-23 mission tended to be somewhat higher than during the two previous missions, ranging from 2.0 to 2.1 in all but the lightly shielded APD-3 location. As on the previous two missions, APD-3 had the highest total dose rate, 375 μGy/d, and the lowest mean quality factor, 1.7. The heavily shielded APD-2 and APD-6 locations measured comparable dose rates of 307 and 304 μGy/d, respectively, and dose equivalent rates of 385 and 323 μSv/d, respectively.

The primary conclusions to be drawn from the FBI-3 internal experiment concern the dependence of dose and more especially dose equivalent on the localized shielding environment surrounding a particular location on the interior of a LEO spacecraft. In general, those APDs which were under heavier shielding tended to measure lower doses but higher mean quality factor, and a greater contribution from high LET particles to total dose and dose equivalent, than did APDs is less shielded locations. These results illustrate the difficulties inherent in providing shielding for a LEO spacecraft. Shielding not only attenuates the primary charged particle flux, but provides a medium in which the primary charged particles can undergo nuclear interactions with the nuclei of the shielding material and thereby produce

secondary particles. The secondaries produced in these nuclear interactions include neutrons and short-range recoil nuclei. Since neutrons lack charge, they interact only with other nuclei and thereby create additional secondary particles. It is only relatively recently that the contribution of neutrons to an astronaut's overall radiation exposure has come to be fully appreciated.

Charged secondary particles, including recoil nuclei and knock-out protons and α-particles, often have an LET higher than that of the primary particles that produce them. This is especially true in the case of the vast majority of trapped protons encountered when a LEO spacecraft traverses the SAA. These high energy protons have LETs significantly smaller than 10 keV/μm and consequently have quality factors of 1. The dose equivalent resulting from ionization produced by these primary high energy protons is equal to the dose. However, the target fragments produced in nuclear interactions between high energy trapped protons and the heavy nuclei of the spacecraft, onboard equipment, and even the bodies of the crew, often possess significantly higher LETs. These high-LET secondaries are in large part responsible lead to the mean quality factors measured aboard Mir being greater than 1. Thus it is the shielding itself that is largely responsible for the elevated levels of dose equivalent and mean quality factor. The effects of shielding on spacecraft are complex with regard to crew dosimetry.

In designing spacecraft shielding, steps need to be taken to minimize the production of high-LET secondaries. Shielding materials are tested by means of radiation transport codes which model the propagation of primary and secondary radiation through the mass and shielding of the spacecraft and determine the resulting dose and dose equivalent. These radiation transport codes include the HZETRN code developed by NASA Langley Research Center[16], the HETC code originally developed by Oak Ridge National Laboratory and adapted for use in evaluating spacecraft shielding by Armstrong et al. of SAIC[17], and the FLUKA Monte Carlo code originally developed by CERN[18]. The dose and dose equivalent measurements made by the FBI-3 experiment serve as a useful series of real-world benchmarks by which to evaluate the validity of these transport codes.

6.2 FBI-4 External Experiment

Dose rate as a function of shielding depth was measured for shielding depths less than 3 g/cm^2 (Figure 29). In both measurements the dose rate was seen to decrease by three orders of magnitude from ~100 cGy/d under 0.01 g/cm^2 LiF shielding to ~0.1 cGy/d under 1 g/cm^2. This rapid decrease in dose rate illustrates the attenuation of the primary particle flux by the initial layers of shielding and has important implications for the design of shielding of EVA suits, solar panels, exterior coatings, and other materials and structures exposed directly to the LEO environment. In the case of EVA suits, a suit of thickness >1 g/cm^2 in all areas is adequate to attenuate the ionizing radiation flux down to acceptable levels for EVA. A suit with less than 1 g/cm^2 most likely will not provide an astronaut with adequate protection during EVA. This measurement also shows the high doses that surface coatings and paints used on the exterior of spacecraft must withstand for prolonged periods of time. The highest energy deposition present in the LEO space radiation environment is within a relatively narrow band of material. This material must be able to withstand the dose rate in addition to large swings in temperature and exposure to UV, on a continuous basis without major degradation.

Effect of the sun's eleven year solar cycle is readily apparent in comparisons of measurements made during the FBI-4 experiment in 1997 during solar minimum and a previous set of measurements made on the exterior of Mir Station in 1991 during Solar Maximum. The FBI-4 measurements were roughly a factor of two less than the calculated Solar Maximum dose rate profile and about a factor of five less than the actual measurements of dose rate as a function of shielding depth made during Solar Maximum. One factor leading to this difference is the temporary trapped radiation belt produced by the 1991 SPEs.

Another factor is the enhancement of the trapped belt fluxes produced during Solar Maximum by the more intense solar wind.

Results from the CR-39 PNTDs exposed on the exterior surface of Mir as part of the FBI-4 experiment are more problematic in their interpretation. While the same rapid decrease in particle flux is seen in the CR-39 data as is seen in the TLD dose/depth profiles, track densities for the more highly shielded (deeper in the stack) layers were not as great as expected. There are a number of possible reasons for this fact having to do with the function of CR-39 in the extreme environment of the exterior of a LEO spacecraft. One possible explanation is that the hermetic seals that were intended to prevent the diffusion of oxygen out of the PNTD canisters did not function properly. CR-39 PNTD needs to be in the presence of oxygen during irradiation and formation of the latent damage trails. A lack of oxygen during track formation can lead to chemical recombination along the latent damage trail, resulting in smaller tracks and a fading in the overall signal. Signal fading can also be caused by elevated temperatures. Like oxygen deficiency, elevated temperatures during and following track formation promote chemical recombination along the latent damage trail, leading to a reduction in track size and a decrease in overall track density. CR-39 layers from the other hermitically sealed capsule will be analyzed in the near future.

Despite this problem, nuclear tracks were readily visible in the CR-39 PNTDs exposed on the exterior of the Mir Station during the FBI-4 experiment as illustrated in Figure 31, and the LET spectrum was successfully measured in the second PNTD layer (Figure 32). The least shielding PNTD layer, under ~0.02 g/cm^2, possessed a track density to high to measure even after chemical process for only 24 hours. The PNTD surface was pitted with a nearly uniform layer of short range particle tracks, mostly from stopping protons. Like the results from the TLD dose/depth measurements, this saturation on the least shielded PNTD and the granular appearance of the post-etch surface give an indication of the energy deposited by the primary LEO radiation environment in a narrow band of material surrounding the spacecraft. After only one 600 μm thick layer of CR-39, particle track density was reduced sufficiently to permit the measurement of LET spectra.

The LET spectrum measured on the second layer of CR-39 PNTD (Figure 32) when compared to the LET spectrum measured in APD-6 inside the Kvant-2 module during the same time period, showed a similar shape especially at higher LETs. Only below ~30 keV/μm was the external LET spectrum significantly greater than that measured in the interior. At 10 keV/μm the external spectrum was roughly four times greater than that of APD-6. It is not know what effect lack of oxygen and elevated temperature play in this comparison. The low LET particles responsible for the external spectrum in this LET region are mostly stopping protons in the SAA. The low energy proton component is rapidly attenuated by the spacecraft shielding and do not penetrate into the interior of the spacecraft.

The FBI-4 results, when grouped with the results from the measurements made on the exterior of Mir in 1991, provide an unprecedented picture of the effect of the sun's eleven year solar cycle on the radiation environment in LEO. Such a set of measurements has never been carried out before on a manned spacecraft. The principle use for the data obtained from the external TLDs and CR-39 PNTDs, in the form of dose/depth profiles and LET spectra, respectively, is in validating the environment models used to calculate the LEO space radiation environment. Principle among these are the AP-8 and AE-8 trapped proton and trapped electron models [19,20]. Measurements made on Mir have already been used to assess the uncertainties in these models [21] and more work in this area is anticipated.

6.3 Overall Conclusions

The joint American and Russian NASA/Mir science program provided an unprecedented opportunity to study the LEO space radiation environment. The Environmental Radiation Measurements on Mir Station

experiment yielded data applicable to a number of different issues of concern to the international space radiation health community. This data is also of use to those groups involved with the long term effects of the space environment on radiation sensitive electronics and materials. Because the Mir occupies essentially the same orbit as that of the International Space Station, results from this experiment are directly applicable to ISS. Results from this experiment expand the U. S. database of radiation measurements in the 51.6° inclination orbit, providing detailed information on the importance of localized shielding.

The successful use of passive radiation detectors for the Environmental Radiation Measurements on Mir Station experiment demonstrate the continued usefulness of such techniques in space radiation dosimetry. The large differences in dose and dose equivalent rates measured by APDs located throughout the volume of Mir during the same mission illustrate the fact that the radiation environment aboard a LEO spacecraft is not uniform, but varies considerably from place to place. Thus a single active instrument, no matter how broad its range of sensitivity, cannot provide a complete picture of the radiation environment throughout the whole of the spacecraft. Similarly, use of TLDs alone cannot provide adequate astronaut dosimetry since high LET radiation is measured with less than 100% efficiency and since TLDs by themselves are incapable of measuring dose equivalent. A radiation dosimeter combining both TLDs and CR-39 PNTDs is capable of measuring the relevant dosimetric quantities, and since these detectors are passive and relatively small they can be deployed in multiple locations throughout the interior of a spacecraft.

The Environmental Radiation Measurements on Mir Station experiment anticipates the ISS Passive Dosimetry System (PDS) to be deployed on the International Space Station in 2001. The PDS, being jointly developed by Eril Research, Inc. and the KFKI Atomic Energy Institute, Budapest, Hungary, combines two instruments successfully deployed on Mir during the NASA/Mir science program. The Hungarian Pille TLD system will be used to provide on-orbit absorbed dose and dose rate measurements while CR-39 PNTDs provided by Eril Research, Inc. will be used to measure LET spectrum. Eril Research, Inc. will then analyze the combined TLD doses and CR-39 LET spectra to determine total dose, dose equivalent, and mean quality factor. Lessons learned during the Environmental Radiation Measurements on Mir Station experiment have played an invaluable role in the successful development of the ISS PDS.

7. References

[1] National Council on Radiation Protection and Measurement (1989) *Guidance on Radiation Received in Space Activities,* NCRP Report No. 98, Bethesda, MD.

[2] Badhwar, G. D. (1997) "The radiation environment in low Earth orbit" *Rad. Res.* **148**, pp. 3-10.

[3] Stassinopolus, E. G. (1988) "The Earth's trapped and transient space radiation environment", in *The Terrestrial Space Radiation Environment and its Biological Effects,* P. D. McCormack, C. E. Swenberg, and H. Bucker eds. NATO ASI Series A: Life Sciences Vol. 154. Plenum Press, New York, pp. 5-36.

[4] Reames, D. (1999) "Solar energetic particles: is there time to hide?" *Rad. Meas.* **30** (3) pp. 297-308.

[5] Badhwar, G. D. and Atwell, W. (1999) "Detailed comparisons of observed dose-time profile of October 19-20, 1989 SPE on Mir with model calculations" *Rad. Meas.* **30** (3) pp. 223-230.

[6] Benton E. R., Benton E. V., Frank A. L., Frigo L. A. and Csige I. (1996), Secondary particle

contribution to LET spectra on LDEF, *Radiat. Meas*. **26** (6), 793-798.

[7] Benton, E. V. and Parnell, T. A. (1988) "Space radiation dosimetry on U.S. and Soviet manned missions," in *The Terrestrial Space Radiation Environment and its Biological Effects,* P. D. McCormack, C. E. Swenberg, and H. Bucker eds. NATO ASI Series A: Life Sciences Vol. 154. Plenum Press, New York, pp. 729-294.

[8] Benton E. V., Frank A. L., Csige I., Frigo L. A. and Benton E. R. (1996), LET spectra measurements on LDEF: variations with shielding and location, *Radiat. Meas*. **26** (6), 783-792.

[9] Benton E. V., Frank A. L., Benton E. R., Armstrong T. W. and Colborn B. L. (1996), Absorbed dose measurements on LDEF and comparisons with predictions, *Radiat. Meas*. **26** (6), 799-806.

[10] Benton, E. R. and Benton, E. V. (1999) *A Survey of Radiation Measurements Made Aboard Russian Spacecraft in Low-Earth Orbit*, NASA Contractor's Report–1999–209256, Marshall Space Flight Center, AL.

[11] Benton, E.R., Frank, A.L., and Benton, E.V. (2000) "TLD efficiency of ^{7}LiF for doses deposited by high-LET particles," *Rad. Meas.* **32** (3) pp.211-214.

[12] Badhwar, G.D., *Measurements of Radiation Dose Rates During the NASA-Mir 2 Mission* and *Measurements of Radiation Dose Rates During the NASA-Mir 3 Mission,* Internal NASA-JSC Reports (1997).

[13] Schoner, W., Noll, M., Vana, M., Fugger, M., Akatov, Yu. A., and Shurshakov, V.A. "Measurements of the distributions of absorbed dose and average LET of space radiation due to the variations of the shielding conditions," proceedings of the *3rd Workshop on Radiation Monitoring for the International Space Station,* Budapest, Hungary, 24-26 March 1998.

[14] Petrov, V.M., Tchernykh, I.V., Benghin, V.V., Kolomensky, A.V., Ivanov, Yu. V., Shurshakov, V.A., Filippychev, S.A., and Lyagushin, V.I. "Dose rate measurements in Mir Core Module compartments: Dose-A1 instrument data and model estimations," proceedings of *the 3rd Workshop on Radiation Monitoring for the International Space Station*, Budapest, Hungary, 24-26 March 1998.

[15] http://www.hq.nasa.gov/osf/mir/mirvis.html.

[16] Shinn, J.L. Cucinotta, F.A., Singleterry, R.C., Wilson, J.W., Badavi, F.F., Badhwar, G.D., Miller, J., Zeitlin, C., Heilbronn, L., Tripathi, R.K., Clowdsley, M.S., and Heinbockel, J.H. (1999) "A radiation shielding code for spacecraft and its validation*" 44th International SAMPE Symposium and Exhibition*, Long Beach, CA, May 23-27, 1999.

[17] Armstrong, T.W. and Colborn, B.L. (1999) *TRAP/SEE code users manual for predicting trapped radiation environments,* Science Applications International Corporation, Contractor Report for NASA/MSFC SAIC-TN-99010.

[18] Aarbio, P. A., Fasso, A., Ferrari, A., Mohring, H. J., Renft, J., Sala, P. R., Stevenson, G. R., and Zazula, J. M. "FLUKA: Hadronic benchmarks and applications" in *Proc. Int. Conf. on Monte Carlo Simulation in High Energy and Nuclear Physics,* MC'93, Tallahassee, FL 1993.

[19] Sawyer, D. W. and Vette, J. I. (1976) *AP-8 Trapped Proton Environment for Solar Maximum and Solar Minimum,* National Space Science Data Center, NASA Goddard Space Flight Center, NNSSDC/WDC-A-R&S 76-06.

[20] Vette, J. I. (1991) *The AE-8 Trapped Electron Model Environment,* National Space Science Data Center, Goddard Space Flight Center, NSSDC/WDC-A-R&S 91-24.

[21] Armstrong, T.W. and Colborn, B.L. (2000) *Trapped Radiation Model Uncertainties: Model–Data and Model–Model Comparisons,* NASA Contractor's Report–2000–210071.